Mediterranean Journal of Basic and Applied Sciences (MJBAS)
Volume 9, Issue 1, Pages 109-141, January-March 2025

Remote Sensing Applications comprising geological and geophysical Data for neotectonic Investigations: A Case Study in South-Central-Egypt

Barbara Theilen-Willige[1*], Ahmed Hamed[2], Mohamed Khalifa[3] & Ahmed Abdelgowad[4]

[1]Retired from TU Berlin, 23683 Scharbeutz, Waldstrasse 11a, Germany. [2]National Research Institute of Astronomy and Geophysics (NRIAG), EL Marsad Street 1, Helwan, Aswan Regional Earthquake Research Center, Aswan, P.O. Box: 152, Aswan, Egypt. [3]National Research Institute of Astronomy and Geophysics (NRIAG), Magnetism and Electricity Department, Helwan, EL Marsad Street 1, Helwan, Egypt. [4]South Valley University, Qena, Safaga Rd, Egypt. Corresponding Author (Barbara Theilen-Willige) Email: Barbara.Theilen-Willige@t-online.de[*]

DOI: https://doi.org/10.46382/MJBAS.2025.9108

Article Received: 12 January 2025 *Article Accepted: 17 March 2025* *Article Published: 25 March 2025*

ABSTRACT

The analysis of the complex, neotectonic movements in the investigation area in southern-central Egypt and the specific dynamics of the moving units with different sizes and velocities is a difficult task. It requires an interdisciplinary approach, especially the integration of remote sensing, geological, geodetical and geophysical data. Geostructural mapping is essential for understanding the structural architecture and tectonic evolution in the study area. Thus, a prerequisite for the detection of neotectonic activity is a systematic inventory of structural features, fault and fracture zones, traces of magmatic activity, and of seismic and geodetic data. Satellite data support the detailed, structural 2D inventory to a large extent. When combing and merging optical and radar satellite images with DEM data, the morphologic properties at the surface can be determined, especially based on 3D perspective views with vertical exaggeration up to 20 x. Thus, fault related structures like push-up ridges or pull-apart depressions along fault zones can be detected. Based on the digitized structural features and traces of fault zones density calculations were carried out. Those areas with the highest densities of prominent fault zones and fault related structures can be assumed to be susceptible to relatively higher geodynamic activity in the past and, when reactivated, up to recent times. Neotectonic movements affect the present day geomorphology. High-resolution satellite images help to differentiate various traces and types of neotectonic activities and to study kinematic processes along larger fault zones, even influencing recent morphodynamic processes such as the drainage pattern or slope failure. Linear courses and parallel arrangements of dry riverbeds, their meanders, and terraces clearly reveal a recent tectonic influence on their development. The identification of the geomorphic signatures of tectonic activity can be supported by the evaluation of morphometric properties of the surface. When calculating the difference between an original digital elevation model (DEM) and the filled DEM in ArcGISPro software, depressions can be identified that might lead to the identification of pull-apart depressions, basins or of rift zones. By extracting steep slope degrees from slope gradient maps and digitizing traces of mass movements based on satellite images, it can be derived where areas are more likely to be prone to slope failure in case of increasing geodynamic activity such as earthquakes with magnitudes > 5.

Keywords: GeoEye; Sentinel 2; Landsat; DEM-Data; Neotectonic investigations; Earthquakes; Geodynamic activities; South-Egypt.

1. Introduction

Southern-central Egypt offers optimal conditions for the research of different structures, fault zones and their different structural expressions and conditions because of the dry desert climate conditions and relatively low human influence on the landscape in extended desert areas (Figure 1). Moreover, in the southern part of Egypt many strategic projects have been carried out such as the High and Old Aswan Dams, Benban Solar plant (the largest solar plant project in the middle east), and Tushka project southwest of the High Dam Lake for developing the area around Tushka depressions [1]. Therefore, due to the above-mentioned reasons this research aims to contribute to the detection, inventory, and documentation of structural features and of fault zones providing information regarding faulting characteristics and tectonic kinematics, especially of traces of neotectonic movements in youngest sediments. Movements within the Earth's crust in the recent past or currently taking place are referred to as neotectonic processes. Neotectonic movements are commonly associated with areas of active seismicity and faulting. (A fault is defined as an active fault when it possesses the following basic attributes: Surface displacement in the current seismotectonic period, probability and tendency of reactivation or regenerating surface displacement in the future, geomorphic evidence of recent activity such as by influence on the drainage pattern or on slope failure and possible concomitant seismicity). Active faults are the result of lithospheric or

crustal deformation caused by the current tectonic stress field, however, resulting as well in the reactivation of older faults, or the emergence of new faults [3]. A fault is considered active as well, if only a few traces of erosion and sedimentation can be observed and if even the youngest sediments are affected by displacements. Evidence for fault activity are typical structural features such as clearly developed pull-apart basins or push-up ridges, that (when crosscutting rock units with known ages) can be used to learn the relatively age of the fault activity.

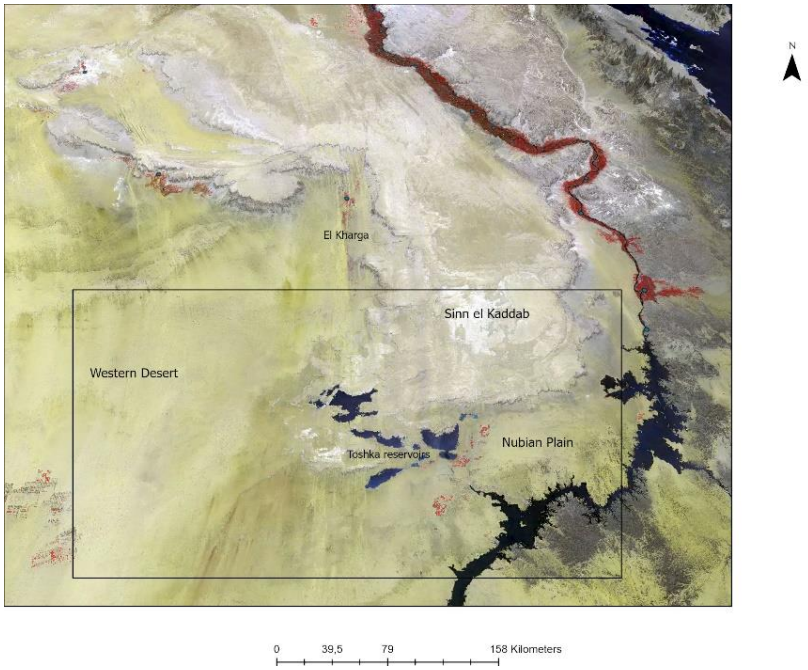

Figure 1. Position of the investigation area in a 3D perspective view.
The Sentinel 2-mosaic was provided by [2].

Another criterion is the evidence of neotectonic movements confirmed by geodetic surveys. Both, earthquake activity and geodetic measurements proving movements, are indicators for ongoing neotectonic activity. Long-term, aseismic, slow creeping movements along fault zones have to be considered as their consequences are often underestimated, but they can cause considerable damage to the infrastructure as well by accumulating stress and effects over time. The inventory of active faults and their risk assessment is an essential contribution to the safety of settlements, land use and infrastructure (railroads, highways, pipelines) and to damage prevention [4] [5].

1.1. Study Objectives

The purpose of this study is to support not only the detection of surface traces of fracture and fault zones, but also areas prone to secondary earthquake triggered effects like horizontal and vertical displacements of rock units or mass movements. Some of the structural features visible on the satellite images seem to trace rifting, rotation and gliding processes. Block motions, displacement of blocks and coupling on the block boundaries can be observed as well. This study aims to contribute to the inventory of these structural features, as far as possible based on satellite data.

Another focus of this study is to draw attention to blind faults / hidden subsurface faults [6], that do not rupture the surface and are covered by unconsolidated sediments, often forming disaggregation bands. Disaggregation bands

are developed in sandy sediments above faults, showing displacements ranging from centimeters to decimeters. Most importantly, their strike closely matches that of known blind faults in the subsurface. As long-wave ALOS PALSAR radar signal can penetrate more than 1 m into loose, dry sedimentary covers, the detection of surface-near faults and disaggregation bands is possible within the radar signal penetration range.

2. Materials and Methods

In the scope of this study the structural analysis will be carried out based on different open-source satellite data (Landsat, ASTER, Sentinel 2, Sentinel 1 and ALOS PALSAR radar data), as well as on GeoEye / OrbView3, Google Earth and Bing Map high resolution satellite images. The evaluations of different satellite data and available geodetic and geophysical data were carried out using the workflow as summarized in Figure 2.

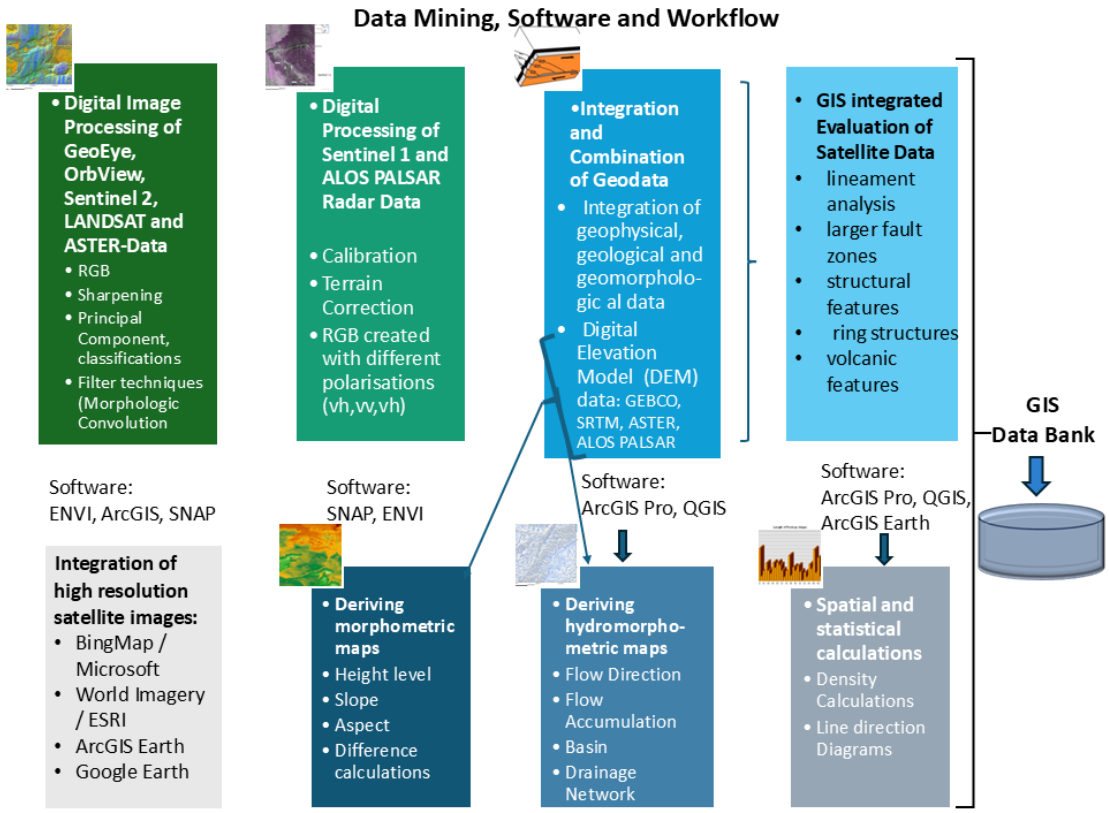

Figure 2. Data mining, software and workflow.

2.1. Landsat, Sentinel 2 and OrbView3 / GeoEye images

The optical satellite data were provided by the USGS Earth Explorer [7], the ESA Copernicus Browser [8], NASA Earth Data [9] and ESA/EUSI [10]. High resolution GeoEye images were provided by ESA in the scope of a project proposal (ESA-Project Proposal-ID, PP0099723, 2024). The latter is part of ESA's Third Party Missions Program, in which ESA has an agreement with European Space Imaging (EUSI) to distribute data products from the mission. OrbView-3 satellite images were collected around the world between 2003 and 2007 by Orbital Imaging Corporation (now GeoEye) at up to one-meter resolution. The OrbView-3 data set includes scenes of one meter resolution (panchromatic, black and white), and of four meter resolution multi-spectral (color and infrared) data.

As digital image processing software served the Sentinel Application Platform (SNAP) / ESA and ENVI / NV5 Geospatial-Software as well as the processing tools integrated into the geoinformation systems ArcGISPro / ESRI and QGIS. The specific digital image processing methods of the different satellite data and image enhancements methods are focused on gaining additional knowledge about the structural pattern such as the filter techniques.

Digital image processing of GeoEye, Orbview, Landsat TM and 8 /9 (the Operational Land Imager (OLI), Sentinel 2 and ASTER data was carried out, mainly by merging different Red Green Blue (RGB) band combinations. Special attention was focused on the creation of RGB images of the Landsat 8 / 9 thermal bands.

2.2. Evaluation of Satellite Radar Images

The radar data were provided by the ESA Copernicus Browser [8], and NASA Earth Data, Alaska Satellite Facility (ASF) [9]. ALOS PALSAR mosaics) were retrieved from the Earth Observation Research Center, PALSAR global mosaic and Forest/Non-forest Map, JAXA [11]. The Advanced Land Observing Satellite (ALOS), Phased Array type L-band Synthetic Aperture Radar (PALSAR) from the Japan Aerospace Exploration Agency (JAXA) provided data with 12.5 m spatial resolution. The Sentinel 1 and ALOS PALSAR radar missions included dual polarization capabilities. By sending out radio waves that bounce off objects and return as echoes, radar creates a detailed picture of the surface. The radar system is able to transmit a signal in a horizontal (h) or vertical (v) polarization and receive in both h and v polarizations. RGB- tools were used here to merge radar images with different polarizations and, thus, get “false-colored” radar images improving the evaluation possibilities, for example by Sentinel 1-vh, vv, vh polarization composites. The different radar wavelengths correlated with the L-Band (23.5 cm) and C-Band (5.6 cm) allow varying radar penetration depths into the surface.

Sentinel 1 Synthetic Aperture Radar (SAR, C-Band, 5.6 cm wavelength), ALOS PALSAR (L-Band, 23.5 cm wavelength) radar data were digitally processed and evaluated. The processing of the radar data was carried out using the SNAP software of European Space Agency (ESA) and the image processing tools integrated in ArcGISPro/ESRI.

The illumination geometry of the radar signals plays an important role for the visibility of the linear and structural features. Those oriented perpendicular to the radar illumination angle appear enhanced, whereas those parallel to the radar illumination are more suppressed, return large amounts of the transmitted energy to the radar satellite sensors (visible in light gray tones), while smooth surfaces scatter the energy and, thus, have low radar returns such as the valley bottoms or aeolian sheets (appearing dark on the radar images). Other factors such as dielectric properties and radar characteristics (frequency, depression angle, polarization) also affect the radar return. As the investigation area is relatively flat radar distortions such as fore-shortening or layover are not evident.

Unfortunately, the use of the method of radar interferometry, that can reveal subtle, horizontal and vertical surface changes, does not make sense in this investigation area because of the high aeolian activity forming dune fields and aeolian sand sheets and, thus, modifying the surface due to sedimentation and wind erosion. Sandstorms with dust and sand loads occur regularly. Rare flash floods with intense sediment transport change the surface topography as well.

Mediterranean Journal of Basic and Applied Sciences (MJBAS)
Volume 9, Issue 1, Pages 109-141, January-March 2025

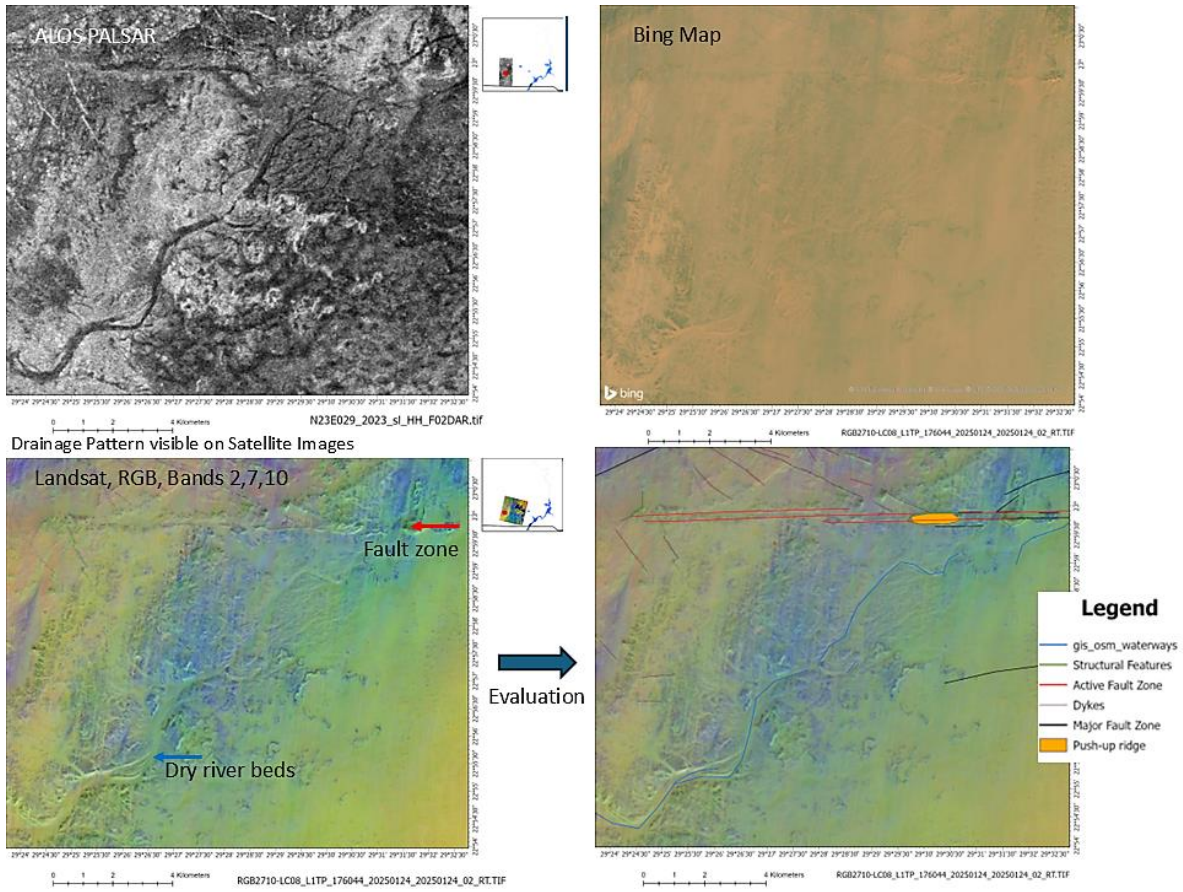

Figure 3. Evaluations of radar and optical satellite images for drainage pattern analysis.

The Bing Map scene shows the area as visible like by the human eye. Youngest sediments are hindering the evaluation. The Landsat 8 scene comprising the thermal bands 7 and 10 shows the aeolian covers and traces of the landscape, whereas the ALOS PALSAR scene provides deeper insights because of the long-wave radar penetration capabilities.

2.3. Evaluation of Digital Elevation Model (DEM) data

Morphometric maps and indicators derived from Digital Elevation Model (DEM) data support the detection of the latest, neotectonic and morphodynamic processes. In order to automatically identify the landform types, the relief elements are grouped into terrain features such as height levels, slope gradients, and terrain curvature. The combination of structural and lithological data with morphometric indicators in a GIS environment is a methodological approach to identify traces of neotectonic movements and resulting structures [12] [13] [14].

Morphometric maps such as slope, hillshade, height level, drainage, and slope maps were generated based on SRTM, ASTER GDEM and ALOS PALSAR Digital Elevation Model (DEM) data using ArcGISPro / ESRI and QGIS digital image processing software. From DEM (Digital Elevation Model) data derived morphometric maps were combined with lithologic and seisomotectonic information in a GIS database.

The drainage pattern is influenced besides the bedrock heterogeneities and morphological obstacles by ongoing geodynamic movements. Drainage systems response to horizontal and vertical deformation in the terrain, which in turn is responsible for variations in channel morphology, sedimentation and erosion processes, and hydrological

characteristics [15]. Deriving the drainage pattern from DEM data supports the detection of subsurface structures. Although the drainage system in the now arid study area was obviously developed during more humid periods in the younger geological past, it traces recent tectonic movements, what can be derived from evaluations of L-Band radar images and Landsat-thermal band combinations (Figure 3) showing extended dry drainage systems. Marine sediment records from the Mediterranean and Atlantic margins have provided consistent evidence of monsoon variability in northern Africa since the middle Pleistocene causing humid periods [16]. Those paleodrainage systems are probably still filled after rare flash floods and modified. Morphological indices such as the valley floor width-to-valley floor height ratio, sinuosity, the asymmetry factor index, etc. as used in other studies [14] to identify the role of tectonics, do not make sense in this study area because of aeolian sand sheets and dune fields and due to the movements of construction materials related to irrigation water management. Because of the Tushka Project and the Southern Egypt Development Project activities a lot of surface material was moved for irrigation systems and canal construction influencing the recent surface water-runoff and infiltration.

DEM data support the detection of fault related structures as well. Pull-apart depressions and basins become visible when subtracting the original DEM data from the Fill-DEM data created in ArcGIS using the Map Algebra tools in the Spatial Analyst extension: The first step comprises the “Fill sink” algorithm from the ArcGISPro software. This procedure fills all depressions in the DEM, including both those generated from data errors (spurious artifacts) and those that record real topographic features. In a second step the sink depths in these areas were extracted by differencing the DEM’s between the sink-filled (“depression-less” DEM) and original DEM. The difference raster map can be used to highlight different types of depressions such as pull-apart basins along active fault zones and to detect smaller, subtle surface features.

2.4. Structural Evaluations

Lineament analysis was an important part of this study. (The term lineament is a neutral term for all linear, rectilinear or slightly bended image elements). Lineaments are often expressed as scarps, linear valleys, narrow depressions, linear zones of abundant watering, drainage network, peculiar vegetation, landscape and geologic anomalies. Linear arrangement of pixels depicting the same color / gray tone were mapped as linear features, as lineaments. They represent in many cases the surface expression of faults, fractures or lithologic discontinuities. When evaluating the satellite data the following components were digitized:

- Mapping of linear features – lineament analysis, analyzing the orientation of linear segments and features in the drainage pattern using the Line Direction tool implanted in QGIS (rose diagrams)
- Mapping of structural features (synclines, anticlines, pull-apart depressions, push-up-ridges, etc.)
- Mapping of linear dykes and ring dykes
- Mapping of craters (used as neutral geomorphological term and description without defining their origin)
- Mapping of plugs and scoria cones

Infrastructural data and water shapefiles were downloaded from [17].

Evidence for fault activity are typical structural features such as step-overs, pull-apart basins or push-up ridges, that (when crosscutting datable rock units) can be used to learn the relatively age of the fault activity. Another criterion is the evidence of displacement during the Holocene and the occurrence of earthquakes along this fault zone. Density calculations of the visible active fault zones, push-up ridges, and craters were carried out in ArcGISPro to derive hints about areas with higher geodynamic activity. Block motions, displacement of blocks and coupling and rifting of the block boundaries can be observed on satellite images as well [5].

Stronger earthquakes have the potential to trigger the development of fault and fracture zones and/or the reactivation of existing faults, not only because of the earthquake shock, but also because of horizontal and vertical movements. Earthquake data were downloaded from different sources such as International Seismological Centre – ISC [18], Euro-Mediterranean Seismological Centre - EMSC [19], USGS) [20], and the epicenters integrated into the GIS.

Another tool for structural research is the analysis of magnetic anomalies. Magnetic anomalies result from geologic features enhancing or depressing the local magnetic field. Variations in the Earth's magnetic field is caused primarily by the uneven distribution of the mineral magnetite in the rocks that make up the upper part of the Earth's crust. Aeromagnetic maps increase knowledge of subsurface structure and composition of the Earth's crust. Global magnetic anomaly grids such as EMAG2 v3 are used for studying the evolution of the lithosphere [21].

3. Geographic and Geologic Overview

3.1. Geographic Setting

Geomorphologically, the study area is a part of the Western Desert, Kharga valley, Nubian Plain, and Sinn el Kaddab Plateau in southern-central Egypt which was subjected to alternative arid and more humid periods leaving their effect on the present land features. The height level of the Sinn el Kaddab Plateau varies from 220 to 550 m above sea level (Figure 4). The recent arid climate is characterized by very low precipitations, interrupted only by occasional, rare, local high precipitations within a short time [22], some of them even causing flash floods and contributing to the development of the visible drainage pattern.

The Sinn el Kaddab- limestone plateau is capped by Eocene limestones, shales, marls, and chalks, exposed in the escarpments. The height levels range from above 500 m in the Sinn el Kaddab Plateau to less than 100 m in the large N-S oriented valleys of the Nile in the east and the Kharga valley in the west of the plateau (Figure 4). Prevalence of present aridity is manifested in the formation of sand dunes, sand sheets, scarcity of natural vegetation and lack of inland surface water [1]. Because of the arid environment aeolian sedimentation and wind erosion by prevailing northern winds are important dynamic elements of the landscape. N-S-oriented, longitudinal dunes and sand accumulations in the wind shadows behind higher areas are clearly visible. Wind erosion created smaller, linear valleys in the landscape in N-S to NNW-SSE direction.

Besides aeolian and fluvial sediments the area is characterized by outcrops of plutonic and volcanic rocks forming inselbergs, craters, and dykes. Dykes and dyke swarms are forming extended narrow ridges in the landscape, oriented mainly in SW-NE and E-W-direction. Numerous simple bowl-shaped or complex craters of different

origins and state of erosion can be observed, partly probably created by volcanic explosions (maars) or mostly by ring dykes. The origin of the clearly visible craters has still to be clarified. Most of the craters are filled with youngest aeolian and fluvial sediments. Volcanic cones and plugs build smaller inselbergs of 20 to 30 m height (Tertiary basalt-dolerites) [23]. Remnants of the Nubian sandstone form inselbergs and flat elevations.

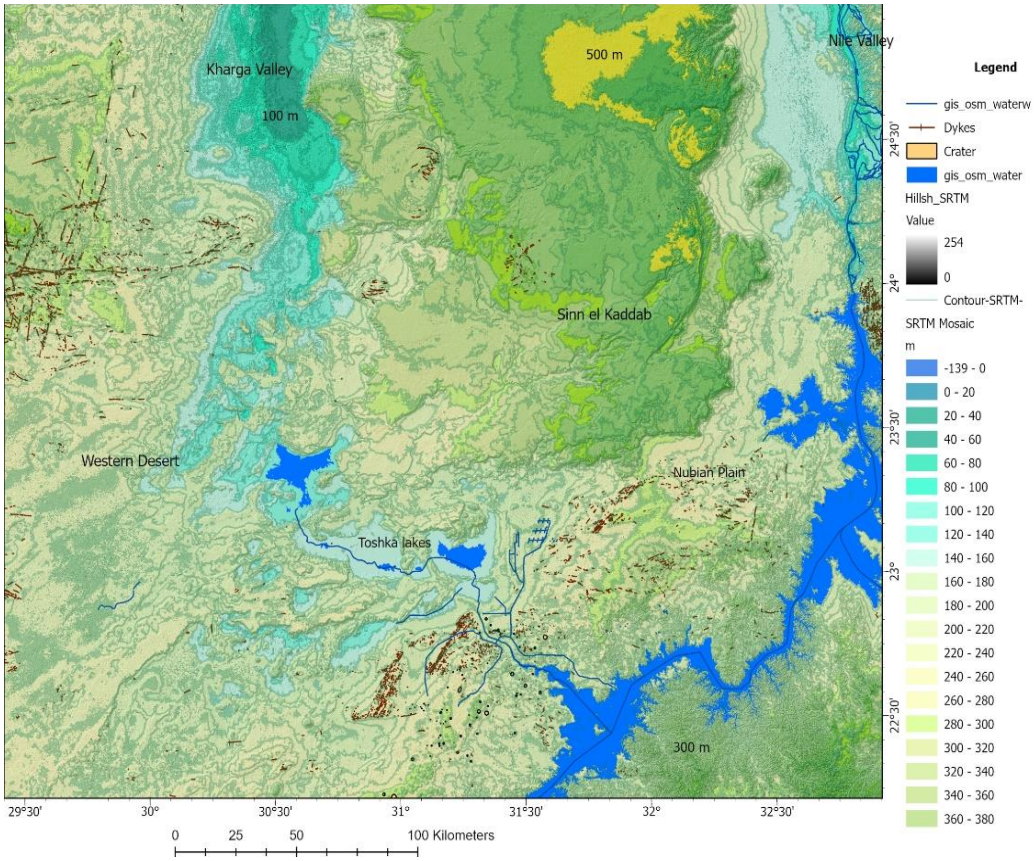

Figure 4. Height levels derived from SRTM DEM data.

3.2. Geologic Overview

The investigation area belongs to the northern part of the African tectonic plate and is a region of a complex geology and a dynamic tectonism, including active seismicity and recent volcanism [24]. These events have resulted in rifting, shear movements, uplifts, volcanic activity, and subsidence throughout the region's geologic history. Africa has been divided in the Eastern Mediterranean into a Nubia plate and a Sinai sub-plate [25]. The Arabian–Nubian Shield represents a collage of intra-oceanic island arc complexes and microcontinental blocks that were assembled as a result of the Neoproterozoic Pan–African Orogenic cycle. Consolidation of arc terranes, emplacement of granodioritic batholites and the formation of the mafic lower crust of the Arabian–Nubian Shield took place between (760–700 Ma), followed by the accretion of composite arc terranes against the western Gondwanaland [26]. In the investigation area several stress fields are overlapping because of the northwestern movement of the African plate, the pressure from the Red Sea rifting zone from eastern direction and uplifting and rotation movements, resulting in a very complex, interacting structural pattern. These different kinematic regimes may be related to temporal or to spatial heterogeneous deformation such as temporally kinematic partitioning of deformation, or temporal fluctuations of the stress field. The Nubian plain is covered by sediments ranging in age

from Upper Jurassic to Quaternary according to [27]. The study region is covered by a sedimentary succession that are subdivided as follows, going from older to younger:

• The Precambrian basement rocks comprising granitoids and granodiorites were subsequently extruded by Phanerozoic dike swarms of different compositions including diabase dikes, sheets and volcanic breccias. The movement of the basement rocks causes the sedimentary strata to stretch or rupture. Furthermore, unconformities were noted both within and across rock units [28]. The uplifting of the basement rocks of the area was accompanied by extensional fault propagation and folding. Ductile and brittle deformation styles are observed [29].

• Upper Jurassic-Lower Cretaceous rocks (Abu Simbel Formation) are developed into sandstone with intercalations of mudstone. The Abu Simbil Formation is mostly made up of sandstone and fine to extremely coarse-grained granules and sands, with a small number of claystone interbeds. It immediately covers the Precambrian basement rocks and rests under the Lake Nasser Formation, making it the oldest sedimentary rock unit in the area under investigation [30].

• The Lake Nasser Formation and the Sabaya Formation are two distinct types of Lower Cretaceous rocks that mostly formed into coarse-grained sandstone with intercalations of shale and clayey siltstone.

• The Kiseiba Formation, which is representative of the Upper Cretaceous, is formed into fine sandstone with intercalations of sandstone, silt, and shale [31].

• A series of clastics and reefal limestone intercalations that are abundant in fossils associated with the Kurkur Formation make up Paleocene rocks.

• The Garra Formation and the Dungul Formation are two distinct types of lower Eocene rocks. They are mostly made up of thick beds of limestone, with some chalky and sporadic siliceous and dolomitic rocks.

• Oligocene rocks are developed into dark low hills.

• Mid Tertiary volcanism is widespread, with successive pulses in the Late Eocene followed by phases related to the opening of the Red Sea and ranging in age from Late Oligocene to Middle Miocene. This volcanism is uniformly basaltic and widely distributed in Egypt and in Sinai. The Quaternary volcanic activity took place mainly in the southwestern desert [32]. Siple and complex craters in the study area are related to this magmatic activity (Oligocene basalts) [23].

• Quaternary rocks are formed into aeolian, lake, and playa deposits in addition to alluvial deposits (Figure 5).

The sedimentary rocks comprise the so-called Nubian sandstone ranging from Cambrian to Upper Cretaceous in age. The Nubian Sandstone is flat lying, relatively unreformed and gently dipping west, while it ranges in thickness from 250 to 400 m beneath the western extent of the reservoir. Shale, clay, and hard ferruginous sandstone make up the Nubian facies. The whole column of sediments unconformably overlies the Late Precambrian basement complex. There are several granitic basement outcrops in the region, ranging in size from a few hundred square meters to tens of square kilometers. The regional basement uplift has played a noteworthy role

in the structural pattern. Large, segmented transform faults are intersecting the Western Desert and the Nubian Plain in Central-South-Egypt, associated with strike-slip motion, stepovers (Figure 5). The Nubian Fault System is interpreted as multi-reactivated intraplate strike-slip deformation zones and the dextral transpression was reactivated in the Late Cretaceous-Early Eocene [33]. These complex fault systems and their co-located domes and basins have formed during different time periods and under varying conditions, often reactivated and superimposing each other.

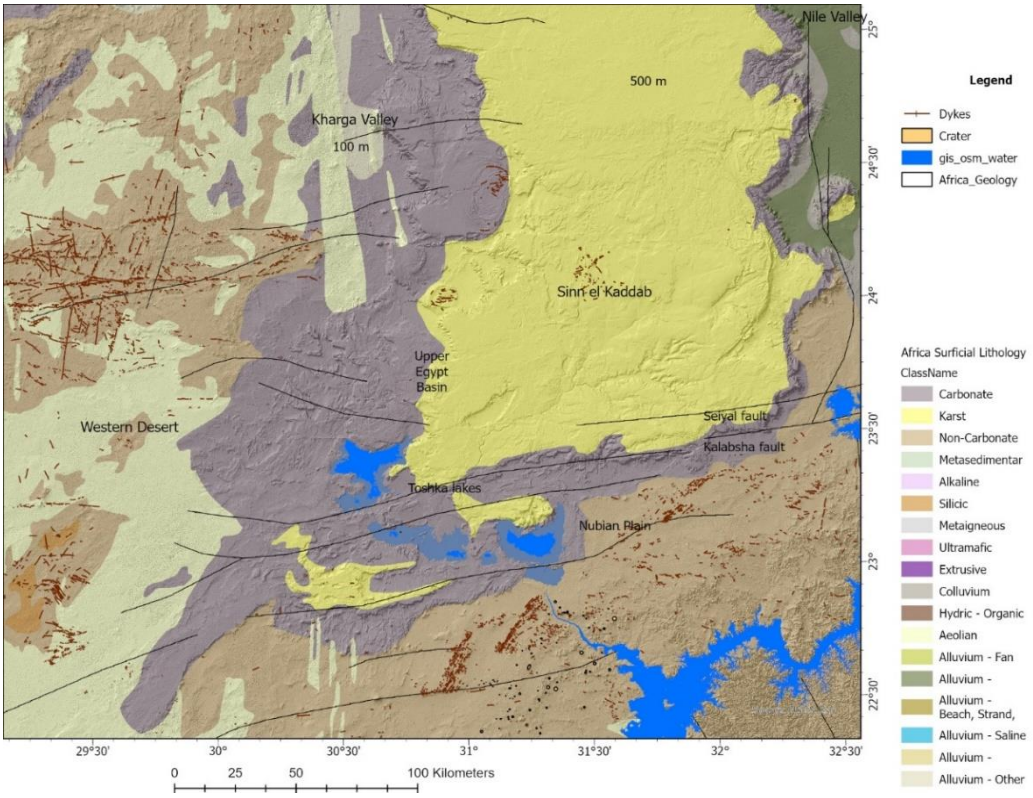

Figure 5. Geologic overview map, data provided by [34] and ArcGIS Online of ESRI: SurfLitho_Africa_USGS_2009.

The E to ENE trending Seiyal Fault extends approximately 90 km westward in the north of the investigation area. The Seiyal Fault has dextral-slip and is associated with en echelon folds [33]. The fault narrows towards the east into relay faults against N to NNE trending faults. The Kalabsha dextral strike-slip fault is another major fault located 12 km to the south of the Seiyal Fault and extends 360 km in an E to ENE direction [34]. It contains four major segments connected with contractional step-overs. The vertical displacement across the fault is 300 m and a reverse-slip component is measured in many parts of the fault course [33] [36]. Towards north of the Seiyal Fault system, another E to ENE dextral-slip fault, which is known as Naqb Dungol Fault, is observed. This fault resembles and has the same characteristics of the parallel Seiyal and Kalabsha faults. In addition, a set of N–S, NNW–SSE and NW–SE trending sinistral-slip faults were mapped [37].

3.3. Seismic and magnetic Setting

Seismically, Egypt's earthquake activity is primarily caused by the movement and contact of the African, Arabian, and Eurasia plates. Both, interplate and intraplate earthquakes, are potentially hazardous [38]. For a long time, the

study area was considered aseismic where no instrumental events were located. In November 14, 1981, an earthquake (Ml 5.3) happened. The epicenter is situated in Lake Nasser's northern most region [39] [39]. The instrumentally recorded earthquakes, including the 14 November 1981 event, are clearly associated with the Kalabsha fault [40] [41]. A local seismic network around the northern part of the lake was installed and the measured data stimulated many researches to carry out seismic studies in order to clarify the seismic situation in that part [39] [42]. These E–Wand N–S fault systems faults are tectonically active by normal as well as strike–slip faulting to different degrees [40]. The earthquake epicenter concentration in swarms and clusters around the reservoirs and dyke swarms and craters are obvious, as well as their position along fault zones. Figure 6 visualizes the occurrence of earthquake epicenters.

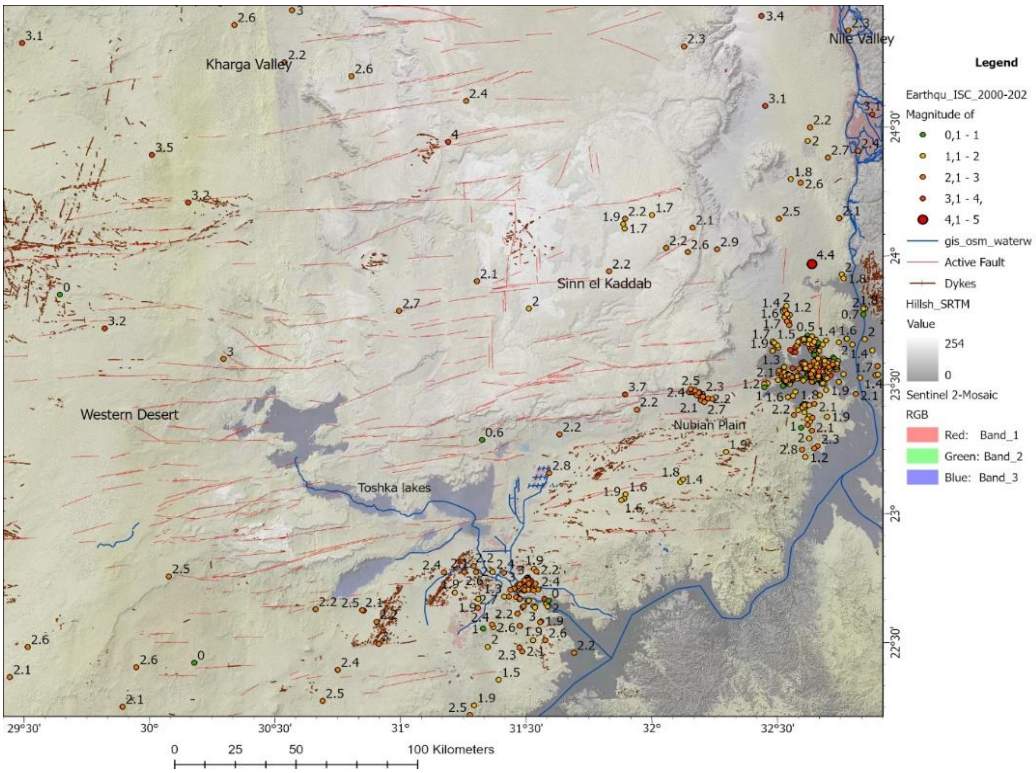

Figure 6. Distribution of earthquake epicenters, earthquake data: [18],[19],[20].

The amount of infiltrating water has an influence on potential earthquakes, when infiltrating into vertical, deep seated fault zones, causing trigger effects. [43] and [44] examined the potential for reservoir-induced seismicity in the triggering of earthquakes that accompany the impoundment of large reservoirs. The filling of large reservoirs changes the stress regime either by increasing vertical stress (loading) or increasing pore pressure through decreased effective stress. In some cases, reservoir-induced seismicity has been observed shortly after the initiation of filling. Several studies have shown a correlation between the temporal distribution of seismicity and the water level variations in Lake Nasser [45]. In general, the water level attains its maximum in November–December and its minimum in July-August. Daily distribution (10 day) histograms of the earthquakes and water level exist for the period (1981–2011). There is no direct relation between the water level and the number of earthquakes, but the Aswan Lake could be triggering earthquakes during this period [40]and, thus, influence neotectonic activities. The detailed inventory of the surface-near fault and fracture pattern might help to detect

those areas, where the permeability of rocks is relatively higher, supporting intrusion and infiltration of surface water after rare, heavy rains.

EMAG2 (Earth Magnetic Anomaly Grid with 2-arc-minute resolution) data support the detection of main structural features. The features and patterns of the magnetic anomaly maps reveal details of subsurface geology including the locations of buried faults, magnetite-bearing rocks, which include many kinds of rocks of interest to mineral exploration and environmental studies, and thickness of surficial sedimentary rocks. Unfortunately, only parts of the investigation area were covered by EMAG2 data provided by [21], (Figure 7). Nevertheless, the distribution and contours indicate WSW-ENE and SSW-NNE oriented trends following the structural pattern in the subsurface.

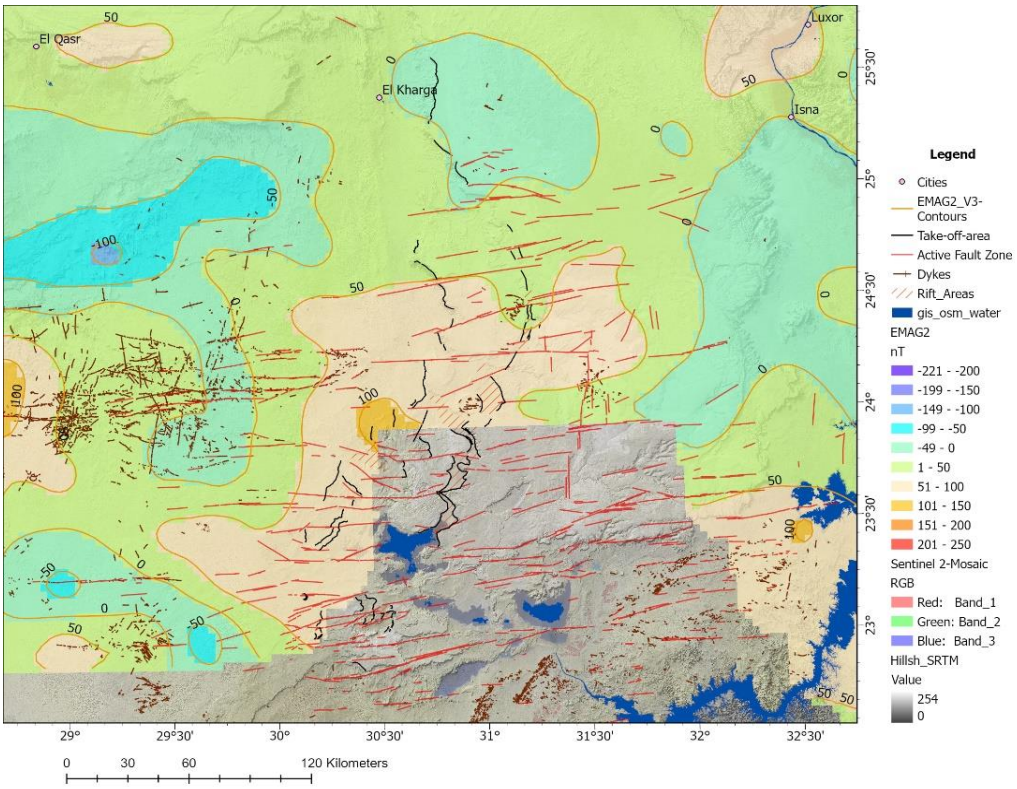

Figure 7. EMAG2- Earth Magnetic Anomaly Grid scene of the investigation area.

4. Results

The presentation of the results is subdivided according to the data sources used.

4.1. Evaluation of optical Satellite Data for the Detection of Fault Zones and Fault related Structures

The definition, classification and mapping of active faults are important bases for evaluating their risks for the environment such as compaction or liquefaction along the major faults near the reservoirs, development of ground fissures, vertical and horizontal displacements and groundwater flow changes. Surface displacement and ground subsidence can be caused as well by creeping faults.

As active fault zones were mapped those fault zones visible on the satellite images of southern Egypt that show distinct fault related structures and traces of displacements even in the youngest sediments, supporting the

assumption that there are partly ongoing movements. When dealing with the detection of traces of neotectonic movements, the as detailed as possible mapping of fault zones, their different appearance and fault related structures as shown schematically in Figure 8 is essential. Examples of fault related structures are presented in Figure 8 and Figure 9. Of course, the specific, local lithologic and geomechanically properties of the host rocks have to be taken into account. There are outcrops of magmatic bodies of different composition, age and types in the study area. Due to the intrusion of magmatic bodies, probably mainly of Tertiary basalts, modifying the mineralogic and structural setting of the host rocks (contact-metamorphosis, up-doming, block building, etc.), larger fault zones and fault related structures are less expressed on the satellite images of this area, contrary to those in the relatively undisturbed sedimentary rocks in the environment.

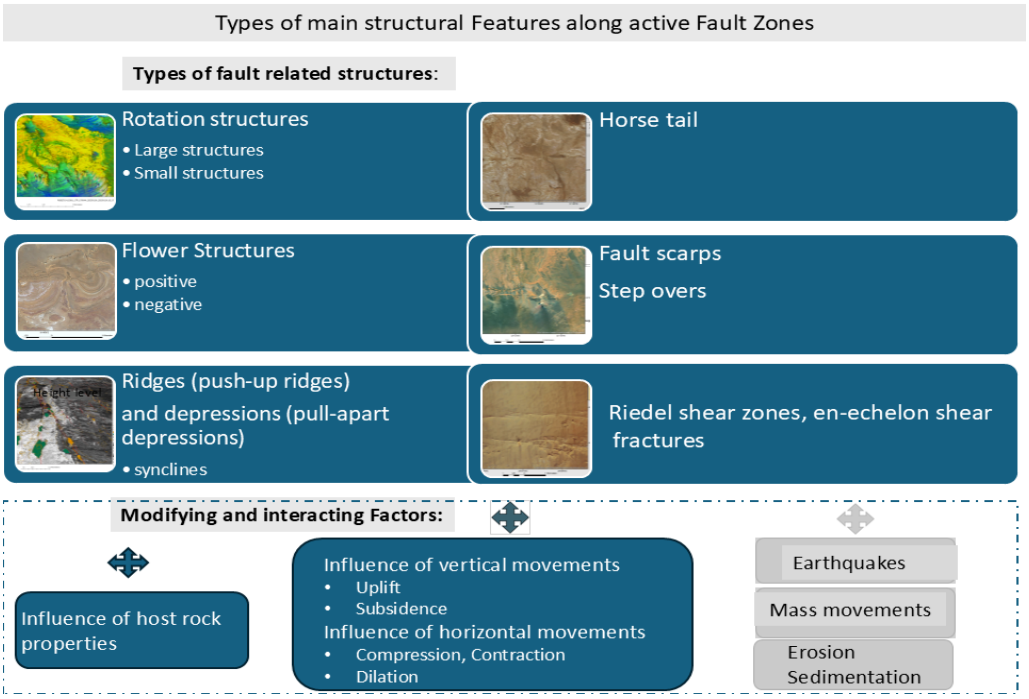

Figure 8. Main fault related structures [4] [5], modified.

The segmented fault systems subdivided in regional transpressional regimes at restraining bends and transtensional regimes at releasing fault bends, responsible for distinct topographical features. These include the formation of push-up ridges at restraining bends and pull-apart basins at releasing bends [40] [47] [48] [49].

The overprinting of different tectonic phases/stages deforming the exposed and unexposed lithologic units is an important issue. Strike-slip duplexes may be compressional or extensional, depending on whether they formed at an extensional (facing towards the movement direction) or contractional (facing against the relative movement) bend. Thrust or normal-fault duplexes accommodate vertical thickening (through stacking of vertical slabs that rise upward and outward over the adjacent blocks) or thinning (through separation of horses). The regional strike-slip faults are often associated with the development of obliquely oriented en echelon arrays of second-order wrench (Riedel) shears, normal faults, and thrust faults or folds [50].

High resolution GeoEye images as demonstrated in Figure 10 contribute to the detailed assessment of fault zones, especially when using filter techniques and merging the image processing results.

Mediterranean Journal of Basic and Applied Sciences (MJBAS)
Volume 9, Issue 1, Pages 109-141, January-March 2025

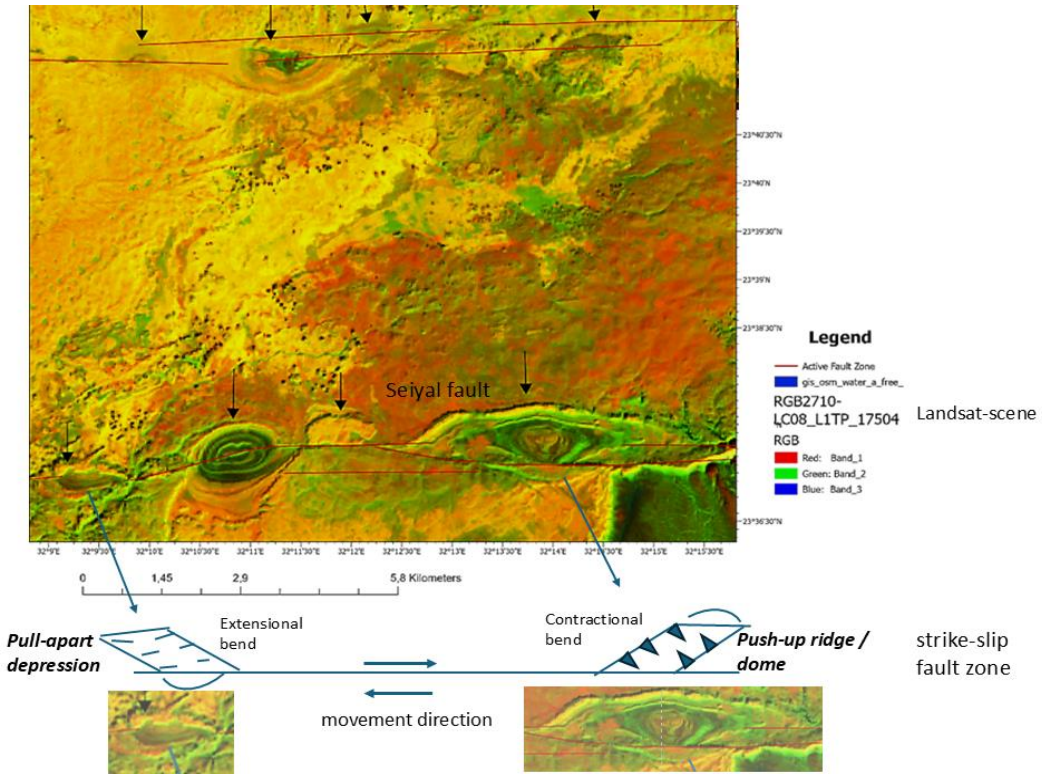

Figure 9. Example of sections of the Seiyal fault (lower fault on the Landsat scene) with fault related structures (sets of isolated rock lenses, often bounded on both sides by parallel segments of the main fault: strike-slip duplexes, synclines, anticlines, pull-apart depressions, push-up ridges see black arrows), sketch: [46], modified.

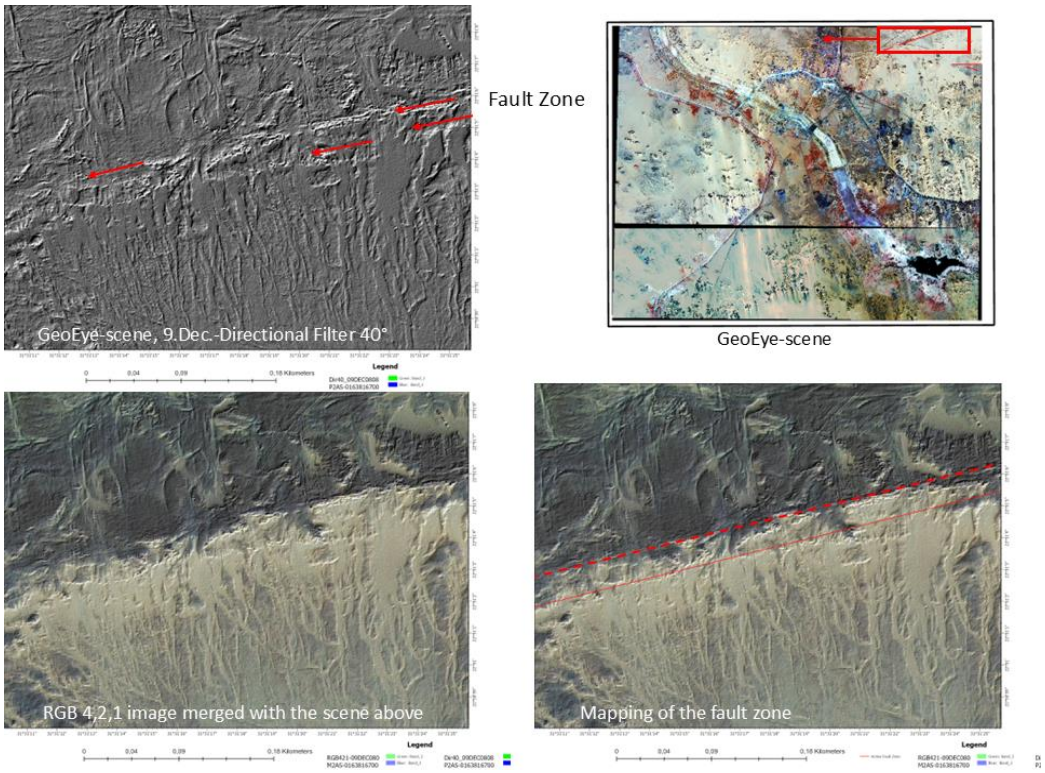

Figure 10. GeoEye-scenes with traces of a larger fault zone striking WSW-WNE.

Merging Landsat thermal bands as RGB image (Bands 2,7,10) with DEM data supports the visualization of fault zones, especially in perspective views. Releasing and restraining bends are complementary features of the

strike-slip faults visible on perspective Landsat image view: The perspective view of the Landsat RGB scene (Figure 11) visualizes the different intensities of movements depending not only on the geodynamic activity (horizontal and vertical displacements), but also on the lithologic and geomechanical properties of the host-rocks (sandstones, lime- and dolostones, marls). Whereas the northern dextral strike-slip fault zone is characterized by aligned push-up ridges comprising smaller anticlines (on the right side of the perspective view, Figure 11), the southern fault zone (on the left side of the perspective view) shows predominantly pull-apart-depressions. Whether this is related to different velocities and intensities of the movements along the fault zones, host rock properties, or other reasons, is still not documented. The slip rates on E-W faults near Lake Nasser are described to be about 0.03 mm/year, N-S faults have lower slip rates, 0.01 to 0.02 mm/year [48]. Traces of rotation structures occur concentrated in areas with outcropping lime-, marl- and shale-stones caused by factors such as clockwise, lateral stress rotations in the surrounding rocks along the fault zones and varying slip rates. Such a larger rotation structure is shown in Figure 12. A 3D perspective view (Figure 13) with a 20 x vertical exaggeration visualizes the complex structure. The relatively older, multi-ringed rotation structure presented in Figures 12 and 13 is intersected and displaced by a relatively younger, right-lateral, E-W-striking strike-slip fault shear zone with a width of about 2 km, that is interrupted by pull-apart depressions, push-up ridges and step-overs. Overprinting relationships can be derived from on the fault intersections.

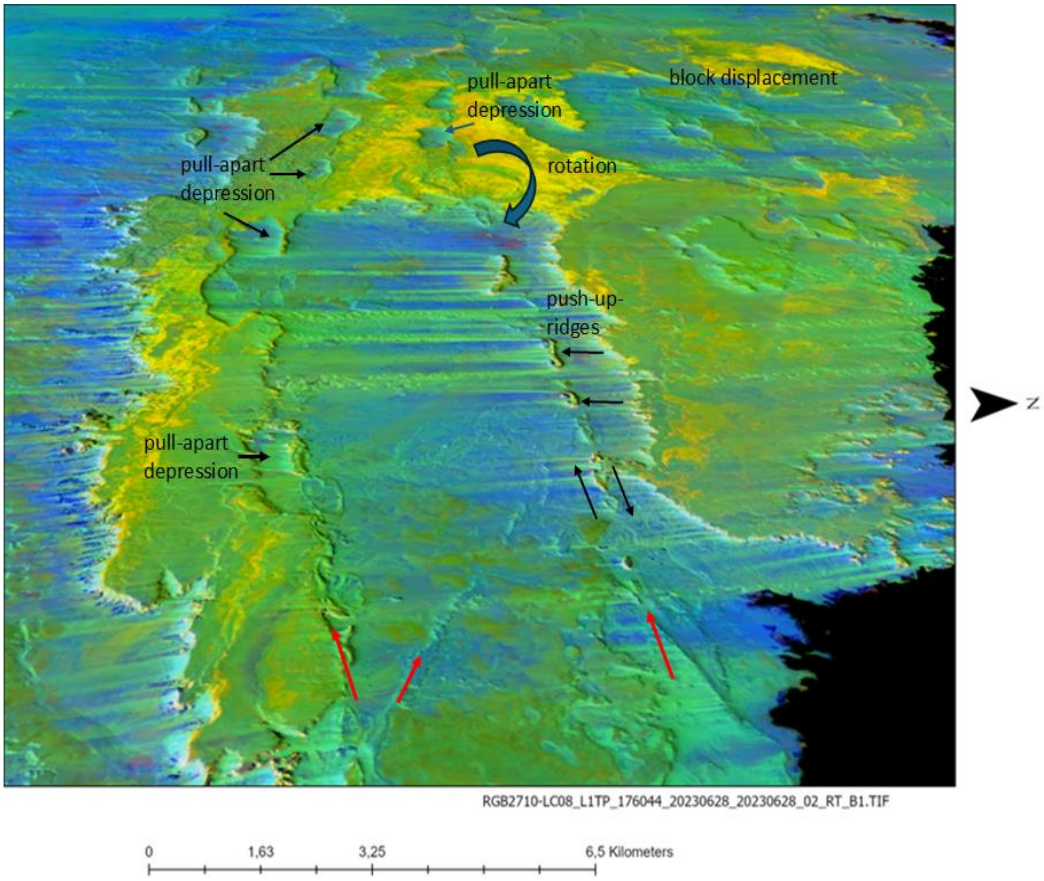

Figure 11. Landsat 8 perspective view (looking towards west) of active strike-slip fault zones (see red arrows) striking E-W with distinct structural features (pull-apart-depressions and basins, sag-ponds, push-up ridges, rotation structures) in the west of the test site. The green stripes are caused by longitudinal dunes and dune fields.

Mediterranean Journal of Basic and Applied Sciences (MJBAS)
Volume 9, Issue 1, Pages 109-141, January-March 2025

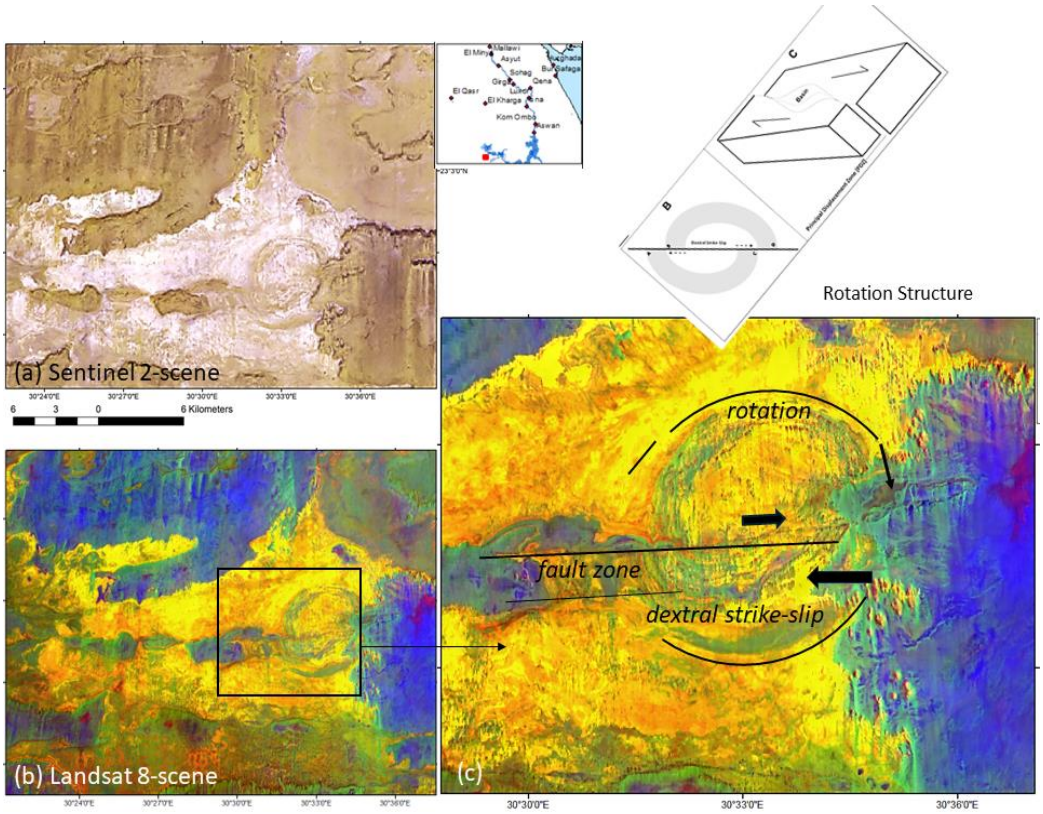

Figure 12. Ring structure dislocated by a shear zone created by rotation processes. Sketch taken from [51].

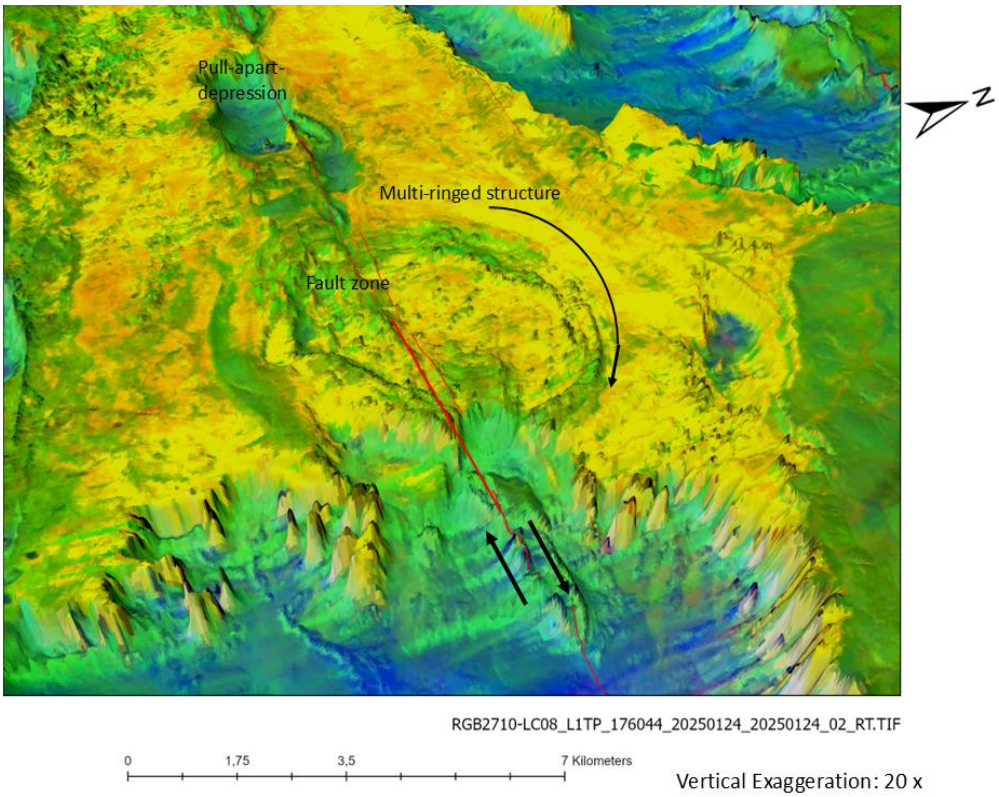

Figure 13. 3D perspective view of the rotation structure on a Landsat scene looking towards West.

Traces of block displacements can be observed on satellite images as well as demonstrated by the next example showing a Landsat 8 (RGB, Bands 2,7,10) scene of probably dislocated blocks that moved towards WSW from the

take-off area with nearly congruent outlines (Figure 14). The relatively morphologic "freshness" of the structures indicating relatively few erosion and sedimentation, support the conclusion that the rifting processes might be recent. (The N-S oriented stripes on the Landsat and ASTER scene are caused by aeolian sand sheets, dune fields and wind erosion.) Of course, the dislocated blocks mapped based on the satellite images have to be verified by field and geophysical investigations to check whether affected rocks are indeed in their position allochthon or still *in situ* (in their original place). May be, there exist even more dislocated and partly clockwise rotated blocks that could not be detected yet on the satellite images.

Mapping of linear anomalies in the drainage pattern developed after rare, intense rains supports the detection of neotectonic movements that are traced even in the youngest sediments. High meander activity is considered as an indicator for tectonic movements [52]. As the area is covered by recent aeolian sand sheets, those loose sediments are predominantly prone to fluvial transport after rain fall. Flash floods with local, relatively high precipitation intensities in this desert area can lead to intense sediment transport and movements within short time. Therefore, the drainage network visible on the high resolution satellite images, is subject to constant minor or sometimes stronger changes, depending on the rain fall intensity. Although the drainage system contains water only during very short time (hours) after precipitations, linear courses, parallel arrangements and abrupt course changes can be observed. The image example (Figure 15) using GeoEye data visualizes the obvious tectonic influence on the drainage development in youngest sedimentary covers.

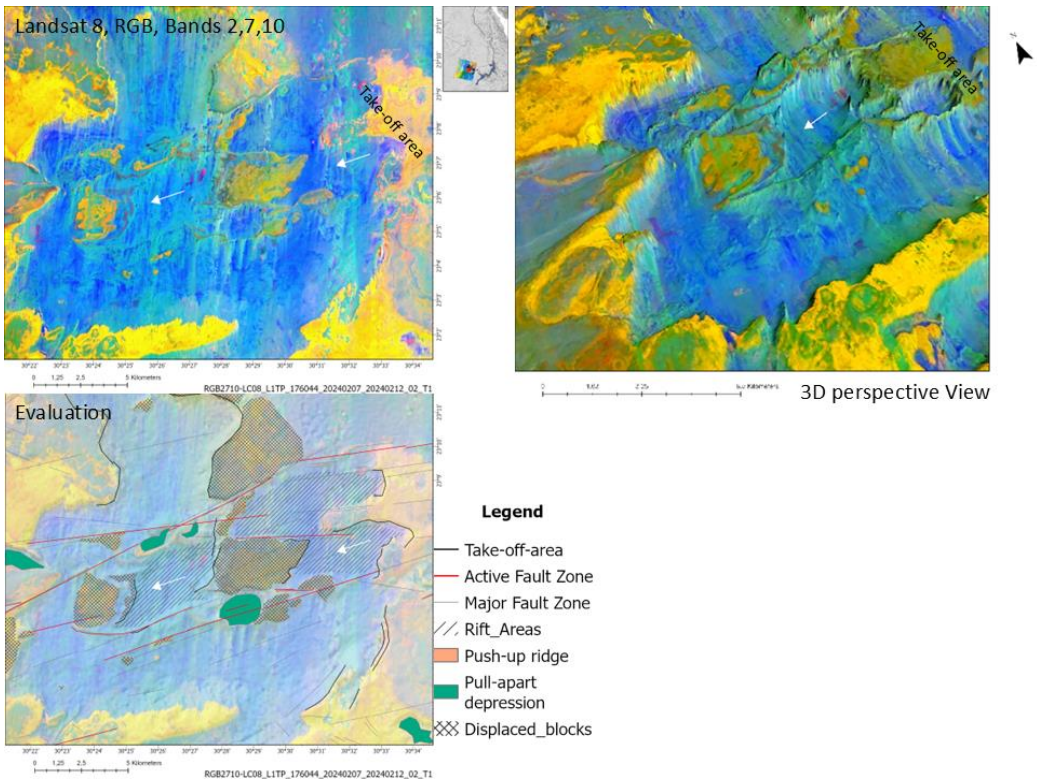

Figure 14. Traces of probable block movements towards WSW visible on a Landsat (RGB, bands: 2,7,10) scene and on a 3D perspective view. The contours of the blocks match in their outline and shape with the outline of the take-off zones in the east. The morphologic "freshness" with little appearance of erosion and sedimentation indicates a relatively recent age of the structures.

Mediterranean Journal of Basic and Applied Sciences (MJBAS)
Volume 9, Issue 1, Pages 109-141, January-March 2025

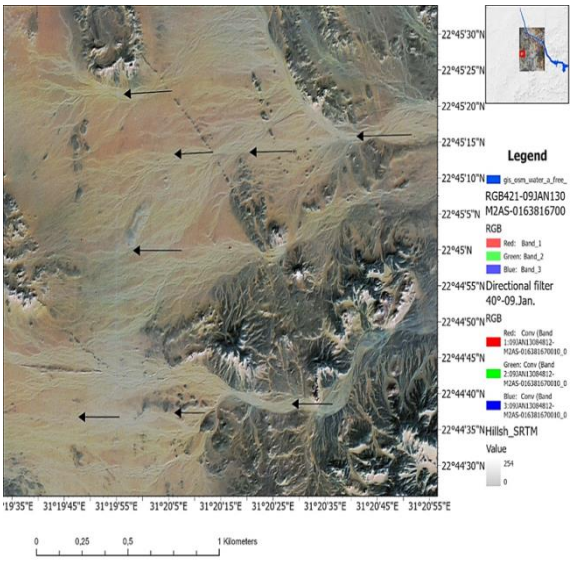

Figure 15. Parallel, linear drainage segments indicating tectonic influence visible on the GeoEye-scene of 09. January 2013.

The parallel, nearly equidistant, linear drainage segments, the sedimentation and erosion pattern in E-W direction indicate a structural influence, and are very likely caused by recent movements. The fact, that linear, parallel courses of riverbeds can be observed, a possible influence of neotectonic movements on the drainage pattern development seems to be obvious.

4.2. Evaluations of Radar Data

ALOS PALSAR images gained in the L-Band (radar wavelength of 23.5 cm) reveal structural information underneath thin sedimentary covers, supporting the detection of active fault zones and traces of ongoing, neotectonic activity. Figure 16 demonstrates as an example an area now covered by the flooded reservoir. Fault related structures become clearly visible. As the area is now partly covered by the reservoir the evaluation of the older radar images before the water cover is helpful for the precise location of the fault zone. In case of stronger, near-field earthquakes, the reservoir might be affected by water and sediment turbulences, especially along the active fault zones underneath. They might reflect, focus or even amplify the effects of seismic waves.

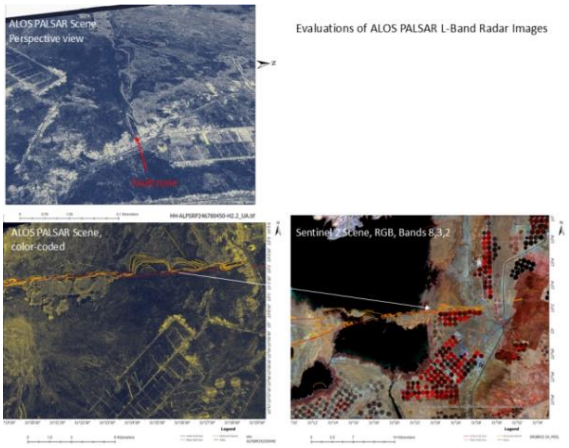

Figure 16. Color-coded ALOS PALSAR radar scene (acquired in 2010 [9]) and Sentinel 2-scene (2024) [8] of the recent situation.

The lineament analysis can contribute as well to the inventory of hidden subsurface faults that do not even rupture the surface and are often covered by unconsolidated sediments, what is demonstrated by the next example (Figure 17). Whereas there are alluvial plains and aeolian covers visible on the Bing-Map and Landsat scene in the area shown in Figure 17, the radar image reveals distinct E-W-oriented linear features that obviously trace faults underneath. Little is known about the thickness of the sedimentary cover. Hidden fault segments can be detected on L-Band radar images whenever they are in the range of long-wave radar penetration. Experiments of [6] provide an additional potential explanation besides radar penetration: The visibility of linear features within aeolian sediments and dune fields on radar images might be explained as the consequence of fabric reorganization by granular flow above active faults, sediments forming so-called disaggregation bands. They develop in unconsolidated, near-surface, sandy sediments.

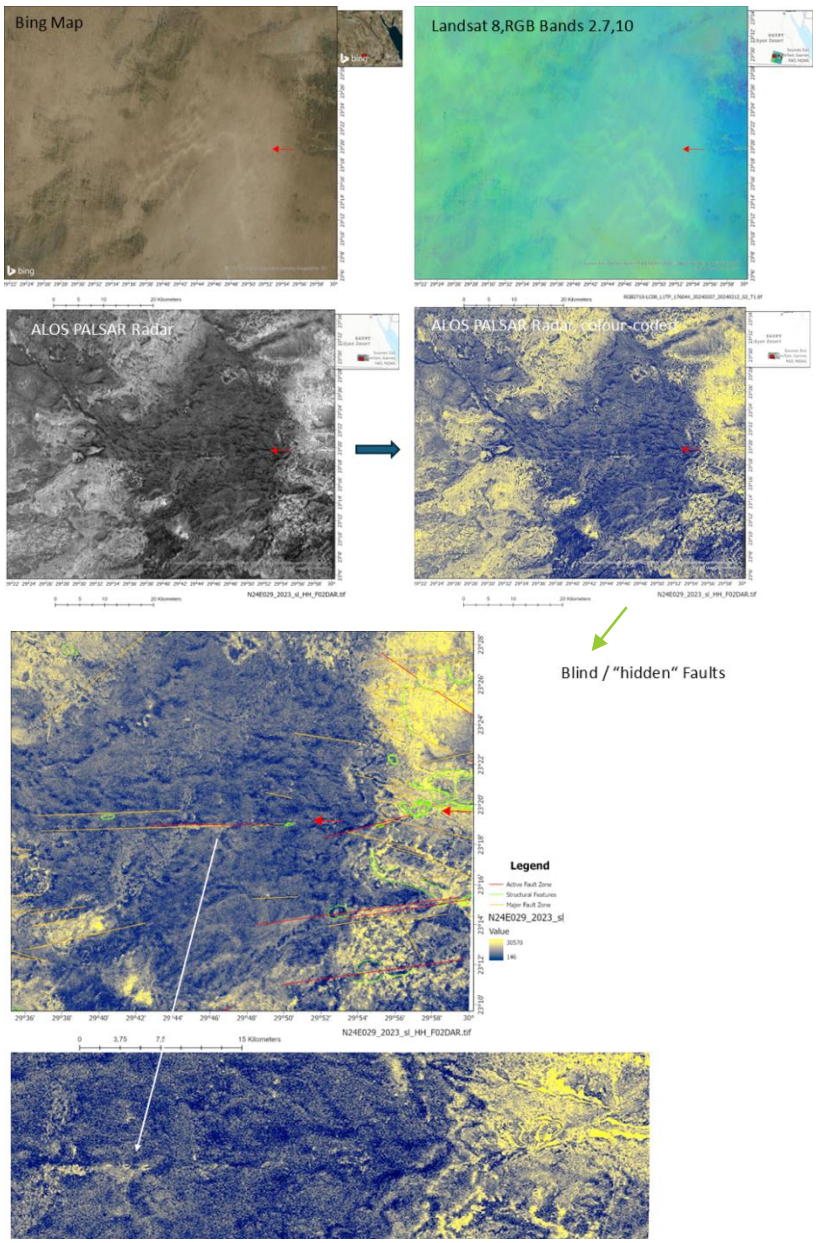

Figure 17. Comparative analysis of BingMap, Landsat and ALOS PALSAR radar data. E-W- striking linear features visible on a colour-coded L-Band radar image are not detectable on optical satellite scenes.

Disaggregation bands are created by shear-related reorganization of the sediment fabric, as a consequence of grain rolling and sliding processes, which can reduce the porosity. Most importantly, their strike closely matches that of blind faults in the subsurface [6].

Radar data such as Sentinel 1 and ALOS PALSAR images support the detection of fault related structures (push-up-ridges, pull-apart depressions) as demonstrated by the next figures (Figures 18 and 19). Especially the L-Band (23 cm wavelength) are very helpful to detect structural details. The radar images often trace more structural details than the optical satellite images because of the capability of radar signals to penetrate loose sedimentary covers.

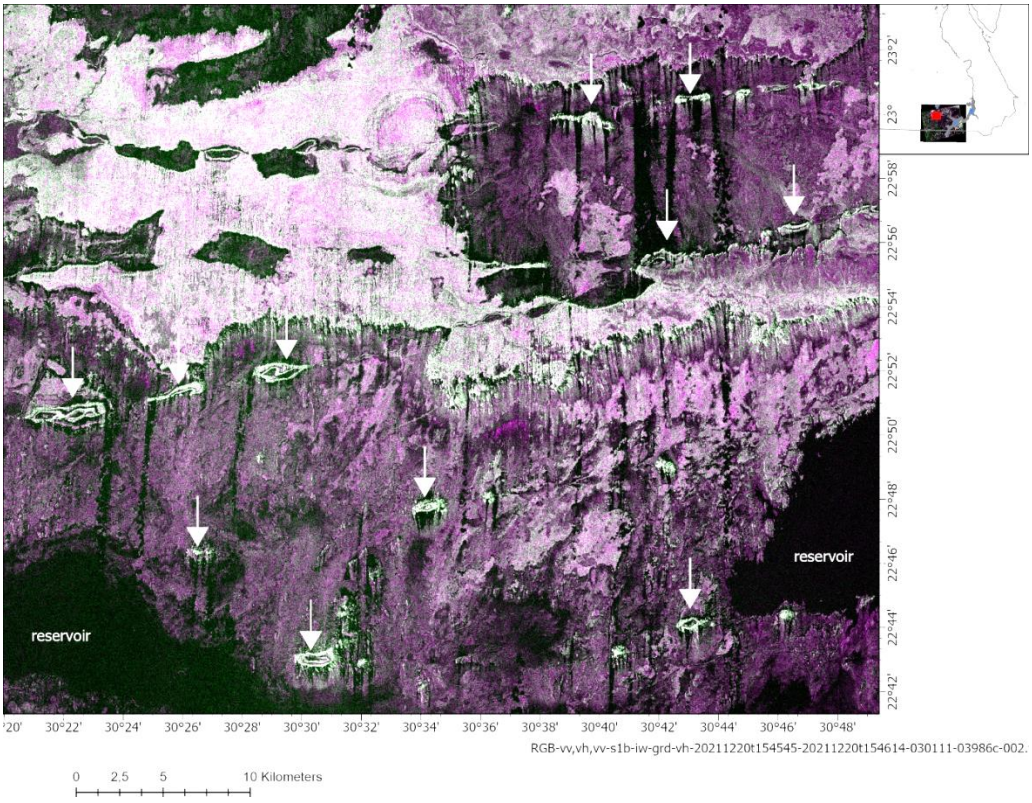

Figure 18. Sentinel 1 RGB scene indication push-up ridges (white arrows) The RGB radar image is the result of the combination of different radar polarizations, providing the advantage of color-coding in comparison with the original radar gray tones.

3D perspective views of ALOS PALSAR radar mosaics from the same area as Figure 18, downloaded from [11], allow the detection of domes, ridges and hills very clearly because of their stronger radar reflection and, thus, appearing in light tones on the radar images), whereas depressions and basins appear black. Most of the depressions, sag-ponds and basins are filled with fluvial and aeolian sediments forming flat and "radar-smooth" surfaces with mirror-like radar reflection and, thus, appearing black.

When combining the radar data with DEM data and using vertical exaggerations (20 x) in ArcGISPro the elongated, oval and "eye"-shaped push-up ridges become clearly visible (see white arrows in Figure 19). Because of the radar penetration into unconsolidated sedimentary covers and the vertical exaggeration, larger fault scarps can be mapped precisely.

Mediterranean Journal of Basic and Applied Sciences (MJBAS)
Volume 9, Issue 1, Pages 109-141, January-March 2025

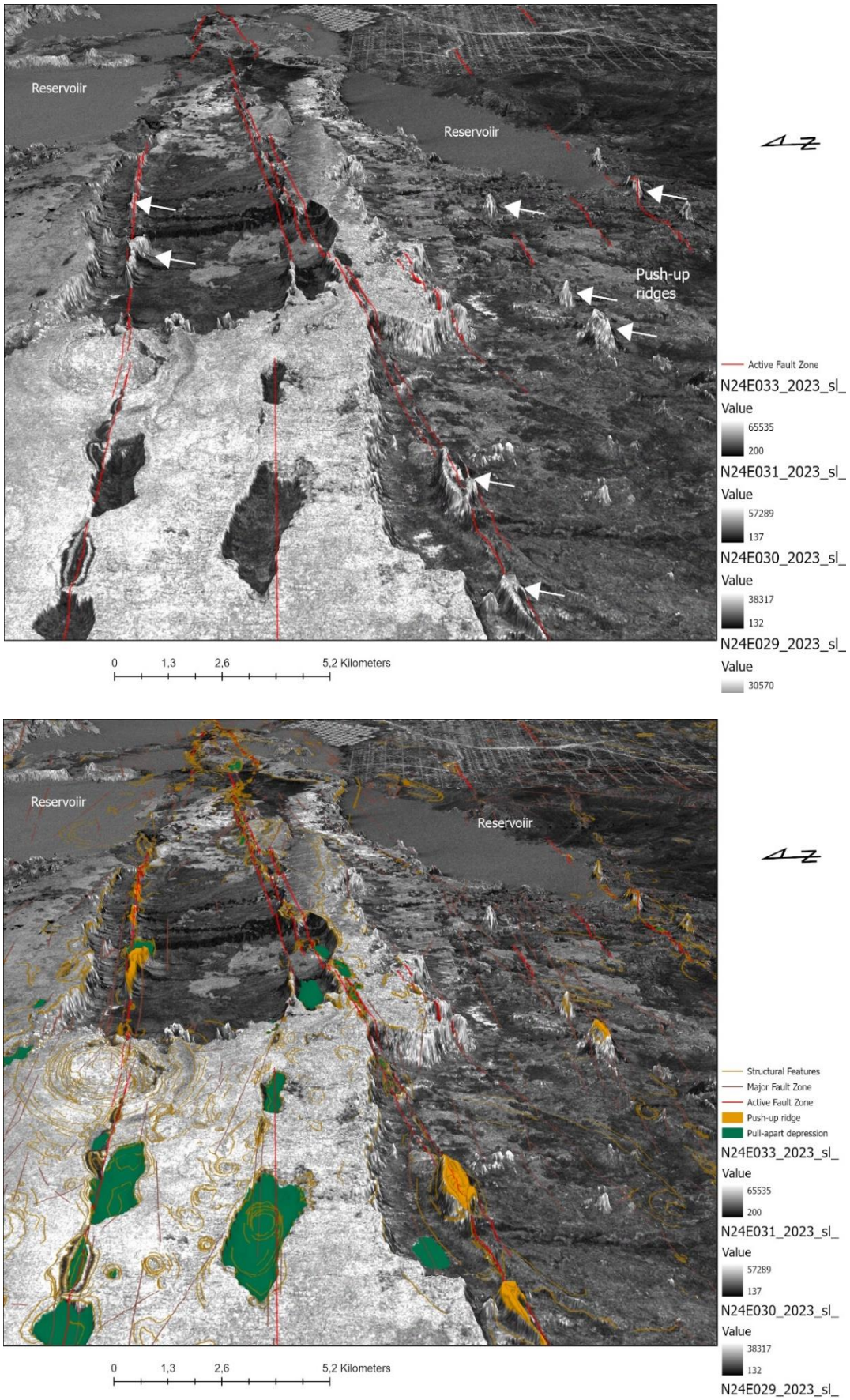

Figure 19. 3D perspective view (13 x vertical exaggeration) of ALOS PALSAR radar mosaics from the same area shown in Figure 18. White arrows indicate the topographic elevations related to push-up ridges.

The digitized structural features of the same area of Figure 19 and that of Figures 10 - 13 are presented in the next Figure 20.

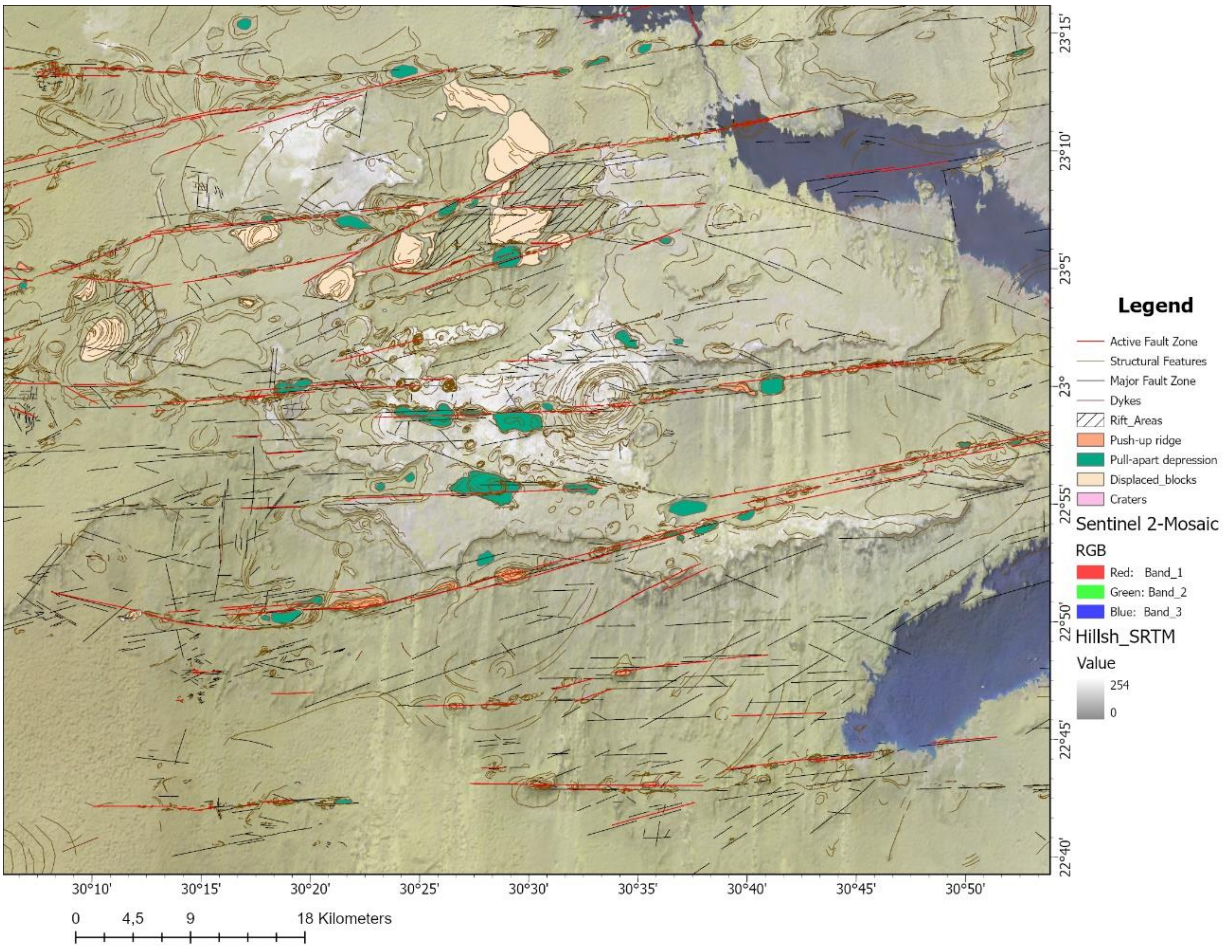

Figure 20. Digitizing structural features.

The intense geodynamic activity in this area might be explained by block-wise up-lifting movements that led to up-doming of the strata, breaking and dislocation of single blocks and their rotations. Strike-slip movements along the active fault zones could have initiated the block-wise displacements as well. Plate tectonic movements cause further stress and strain as the tectonic deformation in the study area is mainly resulting from the interaction between the European and African plates.

The scene presented in Figure 21 is probably tracing a beginning rifting process (indicated by white arrows) as the outlines of the valley borders are nearly congruent. The outline of the eastern border of the complex with the oval- and circular-shaped structures fits very well with the corresponding outline of escarpments along the opposite side of the valley at the western border of the Sinn El Kaddab Plateau like a puzzle piece. This topographic setting with steep escarpment at the eastern flank, a nearly flat bottom and the lower western flank, might support the assumption that the eastern escarpments correspond to take-off zones, where the rifting process started. The processes leading to the development of this valley should be investigated more detailed and are recommended for future research. Differences in the structural pattern are mostly related to stress variations and to the properties of the lithologic units.

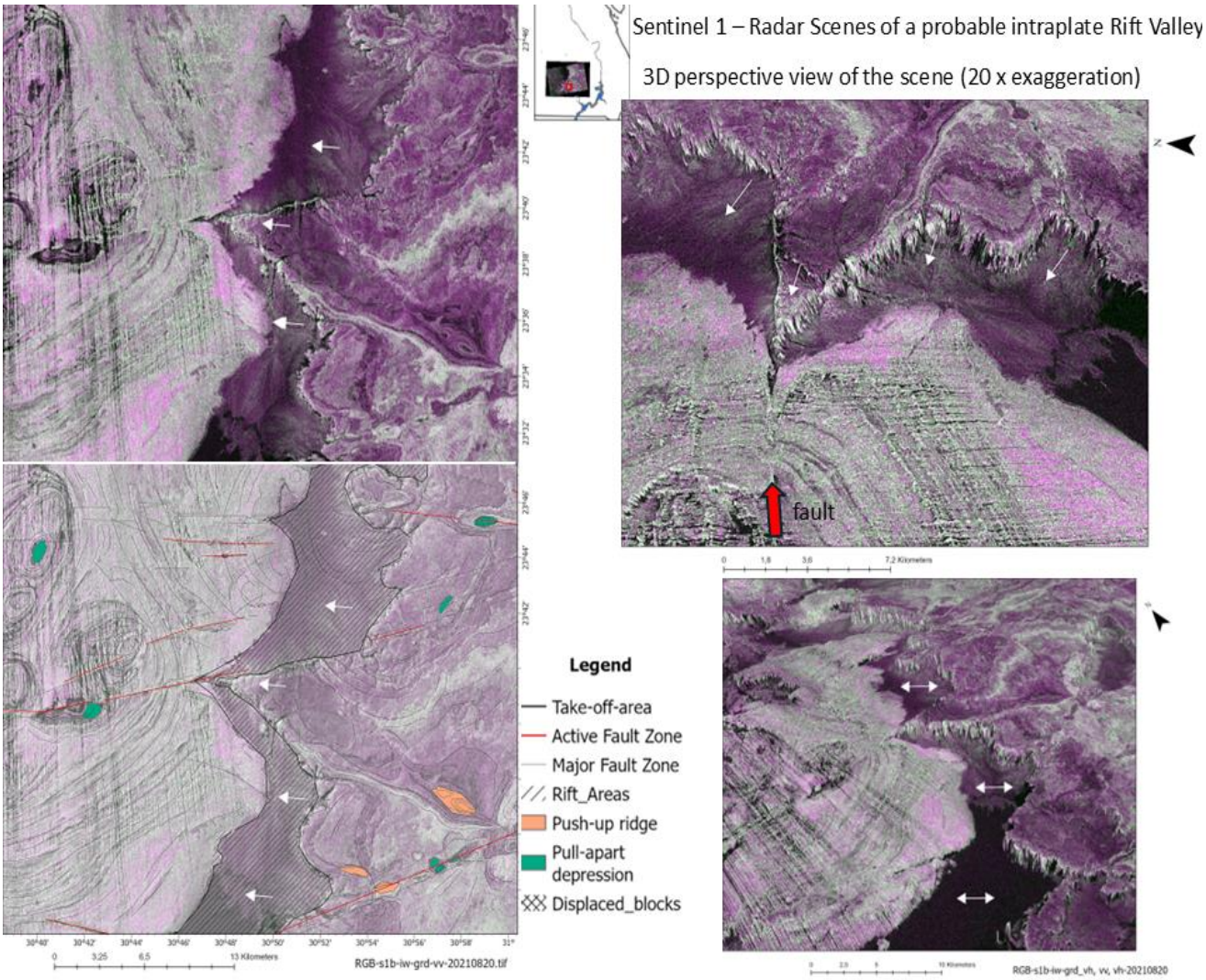

Figure 21. Sentinel 1 radar scene of the probable rift valley with steep escarpments along the eastern border, where the take-off zone of the rifting processes is assumed [5]. The flanks are covered by sediments. The separation was obviously influenced by the movements along the WSW-ENE-striking strike-slip fault at the image center.

4.3. Density Calculations

Based on the line-shapefiles of the "active fault zones" derived from the evaluations of the different satellite images a density calculation was carried out. Figure 22 summarizes the results of the structural evaluations in the investigation area based on the different satellite data. The highest densities can be observed in the west, southwest and south of the Sinn el Kaddab Plateau as well as the Nubian Plain. It can be concluded that the more stress is accumulated in an area, the more fractures, faults and fault related structures occur. The higher density of predominantly E-W striking fault zones might be related to more intense geodynamic activities and movements, whether in the past or until recent remains to be investigated.

Thus, the density calculation helps to identify zones susceptible to higher tectonic stress. However, the complexity of the involved processes (such as different slip rates, influence of earthquakes, interactions with inherited fault systems, or block-wise uplifting movements, etc.) require a more detailed analysis.

Mediterranean Journal of Basic and Applied Sciences (MJBAS)
Volume 9, Issue 1, Pages 109-141, January-March 2025

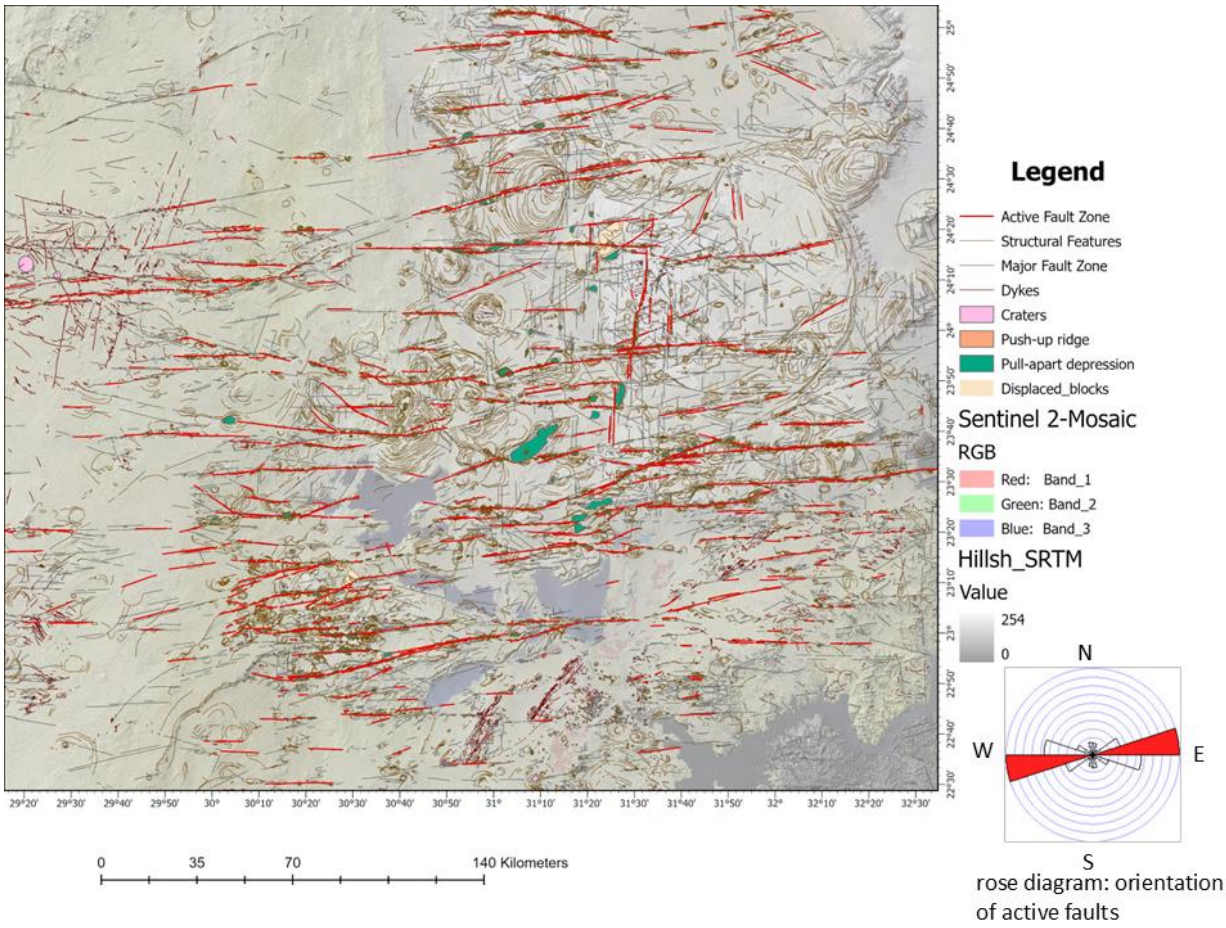

Figure 22. Faults (red lines) assumed to be active fault zones because of their morphologic and structural appearance, and earthquake activity, and their orientations.

In combination with DEM data positive morphological features along active fault zones (fault scarps, push-up ridges forming morphological domes) can be detected based on high resolution satellite data [53]. However, their detailed origin, lithologic composition and structure cannot be derived from satellite images. The push-up ridges / domes with about 1-5 km length and about 2 km width resulting probably from deformations such as flower structures or anticlines were digitized. The average sizes of the ridges are remarkably constant, often forming oval and “eye”-shaped, complex ridges. Their structural development generally results from a shortening component being associated with movement along strike-slip faults [54]. At the center of these topographic-positive features a center-point was placed and density calculations elaborated based on these center points. The density calculation of push-up ridges was carried out, assuming a higher stress and neotectonic activity in areas with higher densities of domes / ridges such as presented in the next figures (Figures 23, 24 and 25).

Of course, the geomechanical properties of the host rocks must be considered. The Nubian sandstones show less pronounced structural features along fault zones than the areas with outcropping shales, marls, lime- and dolostones. In areas with outcropping granitic basement rocks hardly any fault related structural features can be observed. Therefore, it has to be investigated from area to area, whether the density of domes / push-up ridges is more dependent on rock properties and their resistance to deformation or on stress intensities, or on both? The specific, local conditions on the stress pattern can vary small-scaled.

Mediterranean Journal of Basic and Applied Sciences (MJBAS)
Volume 9, Issue 1, Pages 109-141, January-March 2025

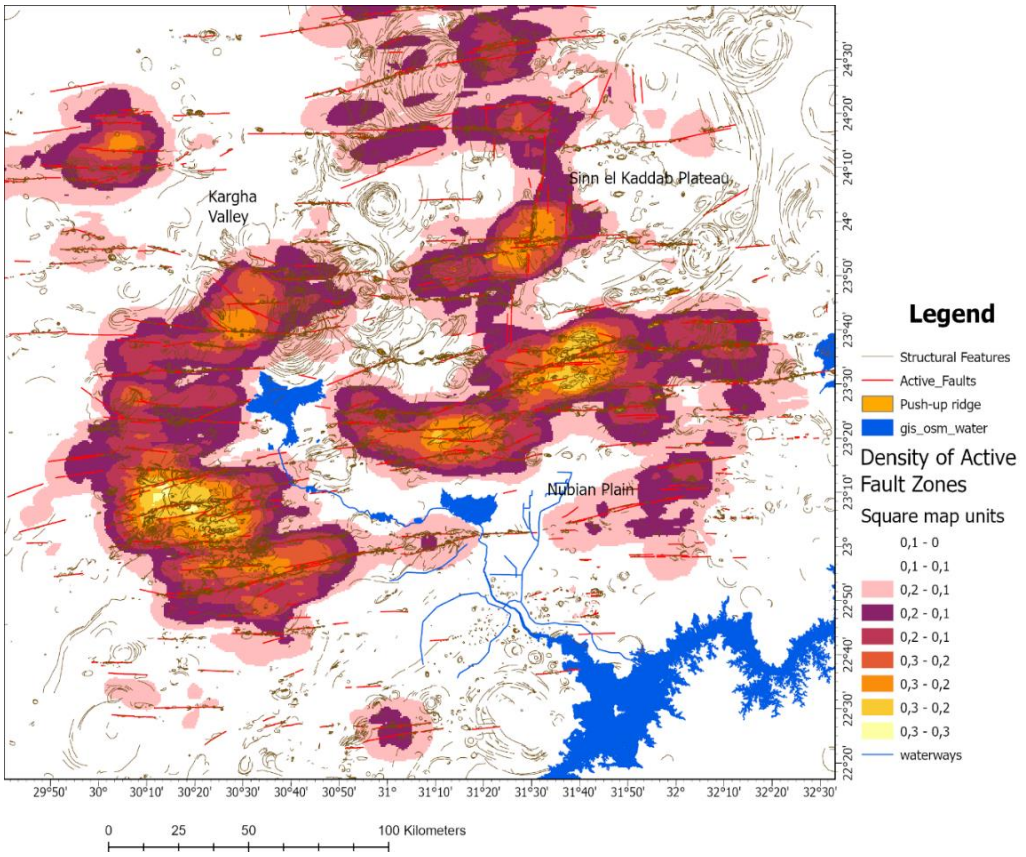

Figure 23. Density calculation of active fault zones.

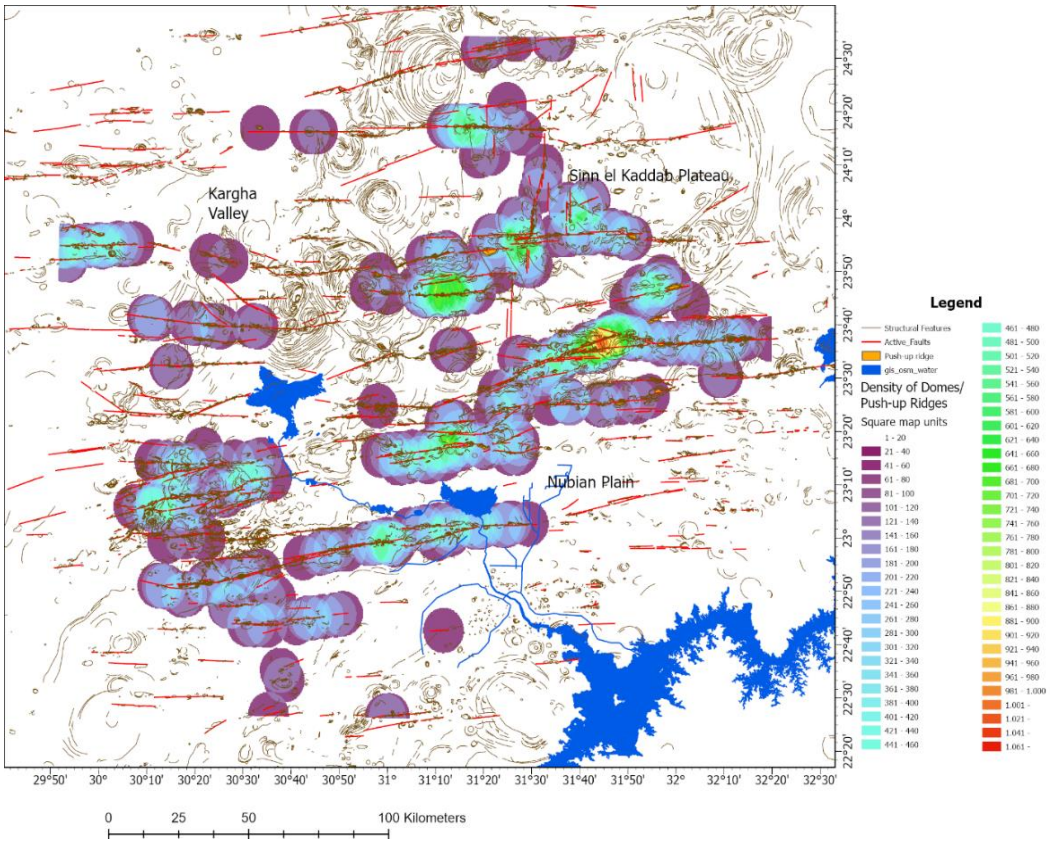

Figure 24. Density calculation of push-up-ridges along fault zones indicating the highest concentrations in the south and southwest of the Sinn el Kaddab Plateau.

When combining the density calculations of active fault zones with the density of positive terrain features as the domes / ridges, it becomes obvious in which areas tectonic movements and their impacts on the outcropping rocks have left traces of stronger, structural deformations. The higher concentration of structural deformations and of fault zones might be related to a more intense geodynamic activity.

Including available earthquake epicenters [18] [19] [20] into these data sets, the concentrated occurrence of earthquake epicenters within the E-W-oriented fault zones seems to be obvious [48] with exception of the earthquake clusters near the reservoirs (Figure 25).

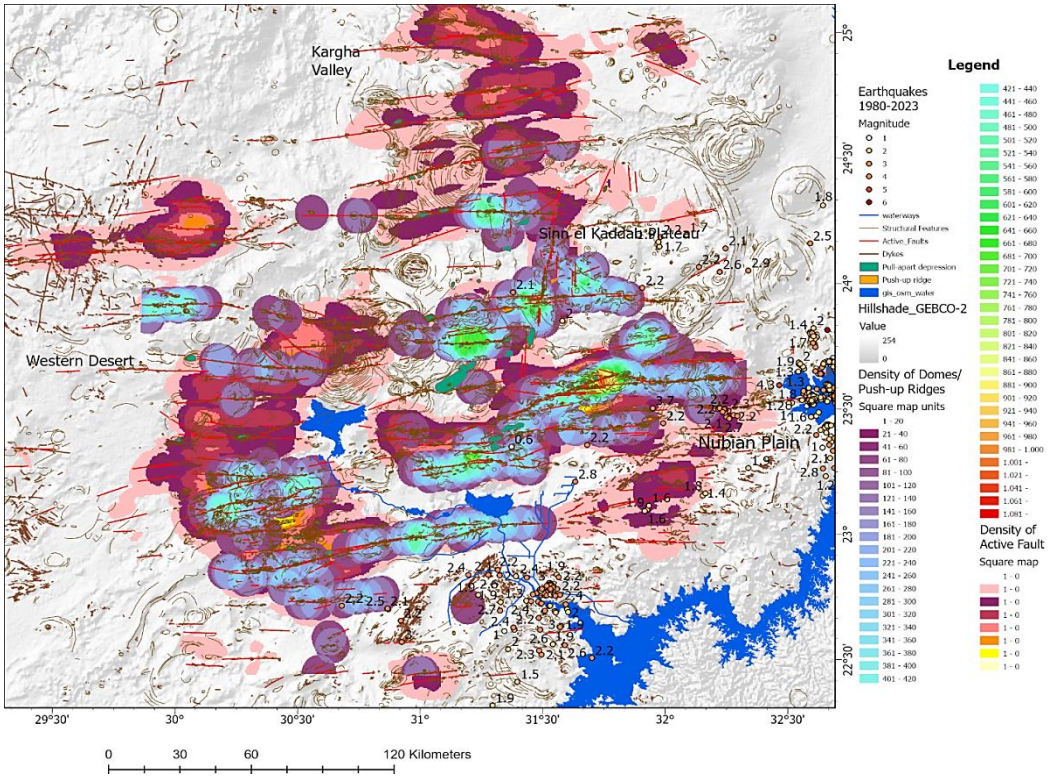

Figure 25. Overview of areas prone to higher densities of active faults and push-up ridges.

4.4. Evaluations of DEM Data

Based on every DEM data set the difference between the original DEM data and filled data was calculated (Figure 26). The processing of the different DEM data (ALOS PALSAR, ASTER and SRTM DEM data) reveals slightly different results because of their different origins (optical satellite and radar data) and spatial resolution and accuracy.

Although the “Fill sink” algorithm from the ArcGISPro software was originally developed to fill all sinks/ depressions in the DEM generated from data errors (spurious artifacts), they reveal as well real, subtle topographic features. The difference raster between the sink-filled (“depressionless” DEM) and original DEM data set highlights different types of depressions such as pull-apart basins along active fault zones or rifting areas. The resulting raster map of Figure 26 shows those areas where the differences of the subtraction of (Fill sinks SRTM-DEM) minus (original SRTM-DEM) occur concentrated. Thus, a better understanding of neotectonic processes related to extensions at releasing fault bends might be achieved.

Mediterranean Journal of Basic and Applied Sciences (MJBAS)
Volume 9, Issue 1, Pages 109-141, January-March 2025

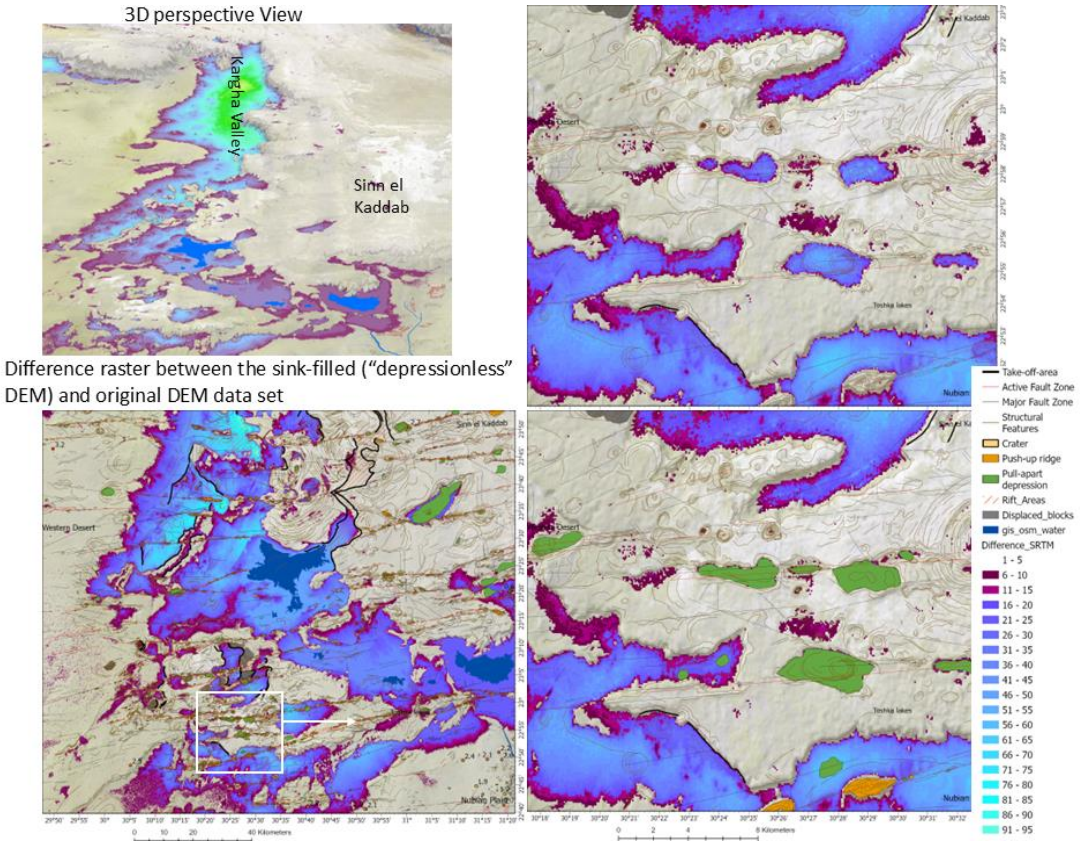

Figure 26. SRTM DEM difference raster map indicating the conformity of differences with pull-apart depressions and basins along shear fault zones.

As the tectonic and lithologic setting plays an important role in the evolution of geomorphic features in the investigation area [55], morphometric properties of the landscape can be used to derive information of neotectonic processes. Of course, the difficulty in the recognition between the geomorphic features that result from surface processes (aeolian and fluvial sedimentation, mass movements) and those that formed by tectonic activity (uplift, subsidence), has to be taken into account. However, when extracting the steep slopes (slope degree > 50° from the slope gradient map derived in this case from SRTM DEM data), it becomes obvious that the steep slopes are related to tectonic activity (Figure 27). Steep escarpments often occur at the borders of pull-apart basins, along fault zones or along take-off zones (caused by lateral, drifting block movements or slope failure). Documented earthquakes near the areas prone to slope failure might have had an influence on the occurrence of mass movements: Block-gliding occurs often along the steep slopes, especially along the Kalabsha-fault and along the high flanks along the western and southern border of the Sinn el Kaddab Plateau where near-by earthquakes and earthquake clusters below 10 km depth were measured. Figure 27 shows the areas with steep slopes in combination with detected slope failure areas on high resolution satellite images as far as possible. As the age of the slope failures is not known, it is not possible to verify yet a connection to recent geodynamic activity. The connection of seismic activity and the occurrence of mass movements, especially after earthquakes with magnitudes > 5, has been documented worldwide (for example: [56] [57]. Further investigation is necessary in the investigation area. By long-term analysis and comparisons of high resolution satellite images combined with geodetic and geophysic data, neotectonic movements and their consequences regarding slope stabilities could then be documented.

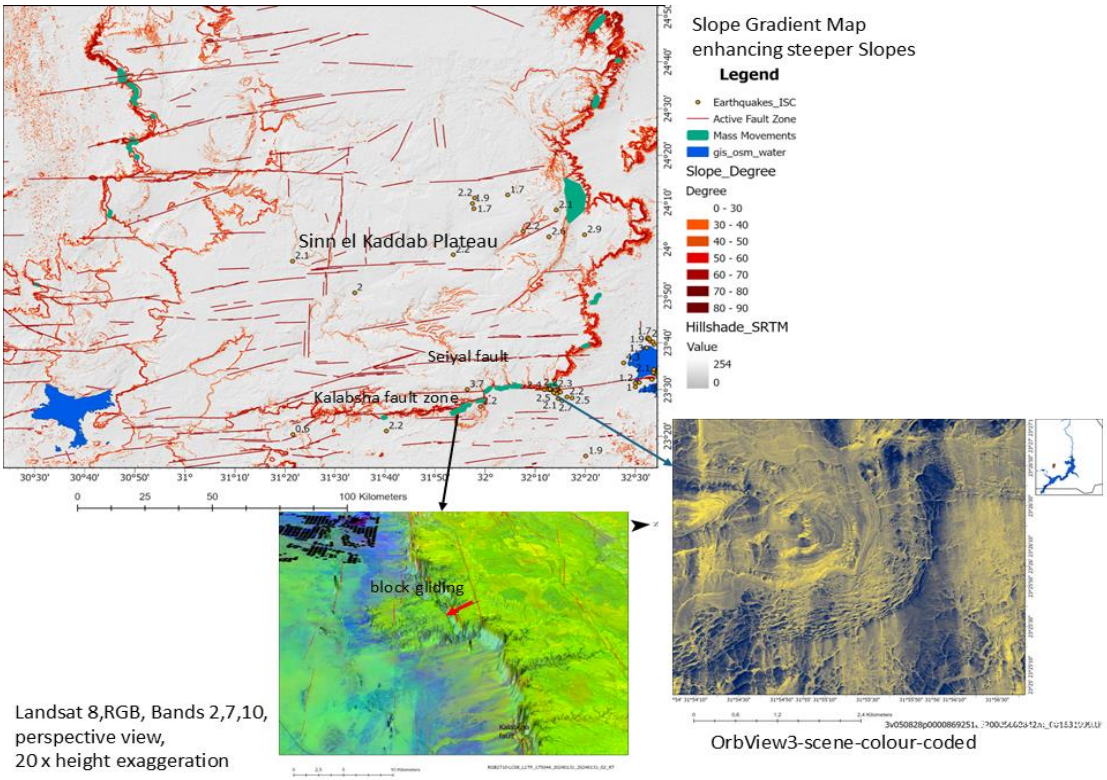

Figure 27. SRTM derived slope degrees > 50° (red) and occurrence of slope failure (green) derived from OrbView3, Sentinel 1 and 2, and Landsat images.

5. Conclusion

Geostructural mapping is essential to understand the architecture and tectonic evolution in the investigation area. Satellite data can contribute to the detection of traces of neotectonic activities by the analysis of morphologic features such as the drainage pattern and slopes, and the inventory of fault zones and of fault related structures. Radar images allow even the detection of so called hidden faults covered by youngest sediments.

High resolution satellite data support their detailed, structural 2D inventory to a large extent. When combing and merging high resolution satellite data (Orbview3, GeoEye) data with DEM data, the morphologic and morphometric properties at the surface can be determined, especially based on 3D perspective views with vertical exaggeration up to 20 x. Calculating the difference between an original DEM and the filled DEM, depressions, the results might lead to the identification of pull-apart depressions, basins or of rift zones.

Density calculations of active faults and of push-up ridges provide hints about areas that might be prone to higher geodynamic activity. It is necessary to comprehensively elaborate the differences in the geodynamic activities and their intensities. The kinematics of the larger fault zones, the development of rotation and folding structures, potential intraplate rifting, and block displacements as well as their ages should be considered for future research. Dislocated blocks mapped based on the satellite images have to be verified by field and geophysical investigations to check whether affected rocks are indeed in their position allochthon or still in situ (in their original place).

Many of fault traces which have been obtained by evaluating the satellite images in the present study, will be surveyed by various and integrated geophysical tools in order to detect their structures, depths and dimensions.

Thus, the main task of remote sensing in this case was pointed out: the identification and consideration of areas and topics for further investigations.

Declarations

Source of Funding

The European Space Agency supported this research by providing high resolution GeoEye satellite images in the scope of the project proposal ID: PP0099723.

Competing Interests Statement

The authors have declared that no competing financial, professional or personal interests exist.

Consent for publication

All the authors contributed to the manuscript and consented to the publication of this research work.

Availability of data and material

The sources of the used data is mentioned in the references. Supplementary information are available from the authors upon reasonable request.

Acknowledgments

The European Space Agency supported this research by providing high resolution GeoEye satellite images in the scope of the project proposal ID: PP0099723. This support is kindly acknowledged. The editorial team of MJBAS and the reviewers are kindly acknowledged for their efforts.

References

[1] Himida, I.H., El Sheikh, A.E., Dahab, K.A., & El Sabri, M.A.Sh. (2009). Application of Modeling Techniques for the Study of Groundwater System in Toshka Area for Sustainable Development. In Proceedings of the 3rd International Conference on Geo-Resources in Middle East and North Africa (GRMENA -II), Cairo, Egypt.

[2] Arab Nubia Group Blog, GIS, Remote Sensing & General, Applications. https://blog.arabnubia.com/.

[3] Wu, Z., & Hu, M. (2024). Definitions, Classification Schemes for Active Faults, and Their Application. Geosciences, 14: 68. https://doi.org/10.3390/ geosciences14030068.

[4] Theilen-Willige, B. (2025). Remote Sensing for Neotectonic Investigations: A Case Study from Southern Egypt. In Gupta, M. (Eds.), Remote Sensing for Geophysicists, Chapter 10: 141–164, CRC Press, Taylor and Francis Group, FL, USA. https://doi.org/10.1201/9781003485278.

[5] Theilen-Willige, B. (2023). Remote sensing and geographic information system (GIS) contribution to the inventory and investigation of dikes in Egypt. Mediterranean Journal of Basic and Applied Sciences (MJBAS), 7(3): 60–84. https://doi.org/10.46382/mjbas.2023.7306.

[6] Brandes, C., Tanner, D.C., Fossen, H., Halisch, M., & Müller, K. (2022). Disaggregation bands as an indicator for slow creep activity on blind faults. Communications Earth & Environment, 3: 99. https://doi.org/10.1038/s43247-022-00423-8.

[7] US Geological Survey (USGS), Earth Explorer, https://earthexplorer.usgs.gov/.

[8] European Space Agency (ESA), Copernicus Browser. https://dataspace.copernicus.eu/browser/.

[9] NASA Earth Data, Alaska Satellite Facility (ASF). https://search.asf.alaska.edu/#/.

[10] European Space Agency (ESA), European Space Imaging (EUSI). https://earth.esa.int/eogateway.

[11] Japan Aerospace Exploration Agency, Earth Observation Research Center (JAXA EORC), PALSAR-2 Global Forest / Non-forest Map "2023". https://www.eorc.jaxa.jp/alos/en/palsar_fnf/data/2023/map.htm.

[12] Sedrette, S., & Rebai, N. (2022). A GIS Approach Using Morphometric Data Analysis for the Identification of Subsurface Recent Tectonic Activity. Case Study in Quaternary Outcrops—Northwest of Tunisia. Journal of Geographic Information System, 14: 94–112. https://doi.org/10.4236/jgis.2022.141006.

[13] Arnous, M.O., Hegazi, A.M., El-Rayes, A.E., & Almoazamy, A.A. (2023). Identification of geomorphic signatures of active tectonics in the Wadi Hagul Basin, Northwest Gulf of Suez, Egypt: insights from SRTM derived geomorphic indices and watershed analysis. Journal of Coastal Conservation, 27: 40. https://doi.org/10.1007/s11852-023-00973-9.

[14] Khalifa, A., Bashir, B., Alsalman, A., & Ögretmen, N. (2021). Morpho-Tectonic Assessment of the Abu-Dabbab Area, Eastern Desert, Egypt: Insights from Remote Sensing and Geospatial Analysis. ISPRS Int. J. Geo-Inf., 10: 784. https://doi.org/10.3390/ijgi10110784.

[15] Sahu, S., Raju, N.J., & Saha, D. (2010). Active tectonics and geomorphology in the Sone-Ganga alluvial tract in mid-Ganga Basin, India. Quaternary International, 227(2): 116–126. https://doi.org/10.1016/j.quaint.2010.05.023.

[16] Paillou, P. (2017). Mapping Palaeohydrography in Deserts: Contribution from Space-Borne Imaging Radar. Water, 9(3): 194. https://doi.org/10.3390/w9030194.

[17] Geofabrik's free download server, Download OpenStreetMap data, http://download.geofabrik.de/africa.html.

[18] International Seismological Centre (ISC), ISC Bulletin: event catalogue search. http://www.isc.ac.uk/isc bulletin/search/bulletin/interactive/.

[19] Euro-Mediterranean Seismological Centre (EMSC), earthquake data. http://www.emsc-csem.org/.

[20] USGS, Search Earthquake Catalog. https://earthquake.usgs.gov/earthquakes/search/.

[21] National Oceanic and Atmospheric Administration (NOAA), National Centers for Environmental Information, Earth Magnetic Anomaly Grid - EMAG2 Survey. https://www.ncei.noaa.gov/products/earth-magnetic-model-anomaly-grid-2/download-data.

[22] NASA, WorldView, EOSDIS. https://worldview.earthdata.nasa.gov/.

[23] Egyptian Geological Survey and Mining Authority (1981). Geologic Map of Egypt, 1: 2 Mio, Cairo, Egypt. https://esdac.jrc.ec.europa.eu/content/geologic-map-egypt.

[24] Saibi, H., Elbarbary, S., & Zaher, M.A. (2024). Geothermal Signatures in North Africa: Examples from Egypt and Algeria. In Hamimi, Z., et al. (Eds.), The Geology of North Africa, Regional Geology Reviews, Chapter 16. https://doi.org/10.1007/978-3-031-48299-1_16.

[25] Özbey, V., Sengör, A.M.C., Henry, P., Özeren, M.S., Haines, A.J., Klein, E.C., Tarı, E., Zabcı, C., Chousianitis, K., et al. (2024). Kinematics of the Kahramanmaraş triple junction and of Cyprus: evidence of shear partitioning. BSGF - Earth Sciences Bulletin, 195: 15. https://doi.org/10.1051/bsgf/2024012.

[26] Ghoneim, M.F., Noweir, M.A., & Abu-Alam, T.S. (2015). Magmatic evolution of the area around Wadi Kariem, Central Eastern Desert, Egypt. Arab J Geosci., 8(1): 9221–9236. doi: 10.1007/s12517-015-1853-0.

[27] Continental Oil Company (CONOCO) (1987). Geologic Map of Egypt, (Scale 1:500,000): (CONOCO), NF 36 NW El-Saad El-Ali, Cairo, Egypt.

[28] Ghoubachi, S.Y. (2012). Impact of Lake Nasser on the groundwater of the Nubia sandstone aquifer system in Tushka area, South Western Desert, Egypt. Journal of King Saud University, Science, 24(2): 101–109. https://doi.org/10.1016/j.jksus.2010.04.005.

[29] Elmagd, K.A., Ali-Bik, M.W., & Emam, A. (2015). Geomorphic Evolution of The Kurkur-Dungul area in Response to Tectonic Uplifting and Climatic Changes, South Western Desert, Egypt. International Journal of Civil & Environmental Engineering IJCEE-IJENS, 15(19).

[30] Klitzsch, E. (1986). Plate tectonic and cratonal geology in Northeast Africa (Egypt/Sudan). Geol. Rdsch., 75(3): 753–768. https://doi.org/10.1007/bf01820645.

[31] Ghoubachi, S.Y. (2004). Comparative Hydrogeological Studies of the Nubia Sandstone Aquifer System in East El-Oweinat and Bir El Shab Areas, South Western Desert, Egypt. Ph.D. Thesis, Fac. Sci., Al-Azhar Univ., Cairo, 303 Pages.

[32] Perrin, M.M., Saleh, A., & Alva-Valdivia, L. (2009). Cenozoic and Mesozoic basalts from Egypt: a preliminary survey with a view to paleointensity. Earth Planets and Space, 61(1): 51–60. https://doi.org/10.1186/bf03352884.

[33] Sakran, S., & Said, S.M. (2018). Structural setting and kinematics of Nubian fault system, SE Western Desert, Egypt: An example of multi-reactivated intraplate strike-slip faults. Journal of Structural Geology, 107: 93–108. https://doi.org/10.1016/j.jsg.2017.12.006.

[34] OneGeology Portal: https://portal.onegeology.org/.

[35] Ali, M., Ali, M.Y., Abdelhady, A., & Fairhead, J.D. (2022). Tectonic evolution and subsidence history of the Cretaceous basins in southern Egypt: The Komombo Basin. Basin Research, 34: 1731–1762. https://doi.org/10.1111/bre.12683.

[36] Earth Resources Exploration – EREX (2005). Surface geology of Upper Egypt: An integrated study of Wadi Kharit, Atmour El Nuqra, Qena Bend, Komombo and Sout Abu Tartur. Internal report Earth Resources Exploration (EREX) (Unpublished).

[37] El Bohoty, M., Ghamry, E., Hamed, A., Khalifa, M., Taha, A. & Meneisy, A. (2024). Surface and subsurface structural mapping for delineating the active emergency spillway fault, Aswan, Egypt, using integrated geophysical data. Acta Geophys., 72: 807–827. https://doi.org/10.1007/s11600-023-01133-1.

[38] Hamed, A., El-Amin, E.M., Abdel Gowad, A.M., & Adly, A. (2025). Seismic hazard assessment for some selected historical pharaonic temples' sites, south of Egypt. Natural Hazards, 121: 2347–2369. https://doi.org/10.1007/s11069-024-06884-8.

[39] Kebeasy, R.M., & Gharib, A.A. (1991). Active fault and water loading are important factors in triggering earthquake activity around Aswan Lake. J. of Geodynamics, 14: 73–85. https://doi.org/10.1016/0264-3707(91)90010-c.

[40] Azeem, M.A., Mekkawi, M., & Gobashy, M. (2014). Subsurface structures using a new integrated geophysical analysis, South Aswan, Egypt. Arab J Geosci., 7: 5141–5157. doi: 10.1007/s12517-013-1140-x.

[41] Hamim, Z., Hagag, W., Osman, R., El-Bialy, M., Abu El-Nadr, I., & Fadel, M. (2018). The active Kalabsha Fault Zone in Southern Egypt: detecting faulting activity using field-structural data and EMR-technique, and implications for seismic hazard assessment. Arabian Journal of Geosciences, 11: 421. https://doi.org/10.1007/s12517-018-3774-1.

[42] Hassib, G.H., & El-Amin, E.M. (2021). Thirty-five Years Investigation of the Reservoir induced Seismicity in and around the northern Part of Lake Nasser, Egypt. Egyptian Geophysical Society, EGS Journal, 19(1): 23–36. https://doi.org/10.21608/jegs.2021.385830.

[43] Simpson, D.W., Stachnik, J.C., & Negmatoullaev, S.K. (2018). Rate of change in lake level and its impact on reservoir triggered seismicity. Bull. Seism. Soc. Am., 108(5b): 2943–2954. https://doi.org/10.1785/ 0120180026.

[44] Simpson, D.W., Leith, W.S., & Scholz, C.H. (1988). Two types of reservoir-induced seismicity. Bull. Seism. Soc. Am., 78: 2025-2040. https://doi.org/10.1785/bssa0780062025.

[45] Mekkawi, M., Grass, J.R., & Schnegg, P.A. (2004). A Long-Lasting Relaxation of Seismicity at Aswan Reservoir, Egypt, 1982-2001. Bulletin of the Seismological Society of America, 94(2): 479–492. https://doi.org/10.1785/0120030067.

[46] Shah, A.A., Bin Yassin, M.N.F., & Bin Haji Irwan, M.I.I. (2017). Is pull-apart basin tectonic model feasible for the formation of Kashmir basin, NW Himalaya. Scientia Bruneiana, 16: 1. https://doi.org/10.46537/scibru.v16i1.27.

[47] Heckenbach, E.L., Brune, S., Glerum, A.C., Granot, R., Hamiel, Y., Sobolev, S.V., & Neuharth, D. (2024). 3D Interaction of Tectonics and Surface Processes Explains Fault Network Evolution of the Dead Sea Fault. TEKTONIKA, 2(2): 33–51. https://doi.org/10.55575/tektonika2024.2.2.75.

[48] Hamimi, Z., Hagag W., Osman, R., El-Bialy, M., Abu El-Nadr, I., & Fadel M. (2018). The active Kalabsha Fault Zone in Southern Egypt: Detecting faulting activity using field-structural data and EMR-technique, and implications for seismic hazard assessment. Arab. J. Geosci., 11: 421. https://doi.org/10.1007/s12517-018-3774-1.

[49] Hamimi, Z., Khalil, M., Saad, H.R., El-Tawapty, M.N., Khamis, H., Elbahrawy, A., & Abdelmaksoud, A.S. (2024). Thrust system, flower structures and transpressive duplexes in Zeidun-Kareim Belt, Central Tectonic Province, Egyptian Nubian Shield (East African Orogen). Scientific Reports, 14: 28814. https://doi.org/10.1038/s41598-024-79864-4.

[50] De Paola, N., & Holdsworth, R.E. (2008). The internal structure of dilational stepovers in regional transtension zones. Geology Review, 50(3): 291–304. https://doi.org/10.2747/0020-6814.50.3.291.

[51] Alam, A., Ahmad, S., Bhat M.S., & Ahmad, B. (2015). Tectonic evolution of Kashmir basin in northwest Himalayas. Geomorphology, 239: 114–126. https://doi.org/10.1016/j.geomorph.2015.03.025.

[52] Burnett, A.W., & Schumm, S.A. (1983). Alluvial river response to neotectonic deformation in Louisiana and Mississippi. Science, 222(4619): 49–50. https://doi.org/10.1126/science.222.4619.49.

[53] Tewksbury, B.J., Mehrtens, C.J., Gohlke S.A., Tarabees, E.A., & Hogan, J.P. (2017). Constraints from Mesozoic siliciclastic cover rocks and satellite image analysis on the slip history of regional E-W faults in the southeast Western Desert, Egypt. Journal of African Earth Sciences, 136: 119–135. https://doi.org/10.1016/j.jafrearsci.2017.06.026.

[54] Nkodia, H.M.D.V., Miyouna, T., Delvaux, D., & Boudzoumou, F. (2020). Flower structures in sandstones of the Paleozoic Inkisi Group (Brazzaville, Republic of Congo): evidence for two major strike-slip fault systems and geodynamic implications. South African Journal of Geology, 123(4): 531–550. https://doi.org/10.25131/sajg.123.0038.

[55] Zaher, M.A., Saadi, N.M., & Watanabeb, K. (2014). Geological applications potential of DEM, ETM+, and gravity data in arid and semi-arid regions with special reference to south- western Desert, Egypt. Arab J Geosci., 7(5): 1705–1716. https://doi.org/10.1007/s12517-013-0847-z.

[56] Xu, Ch. (2014). Preparation of earthquake-triggered landslide inventory maps using remote sensing and GIS technologies: Principles and case studies. Geoscience Frontiers, 91(6): 1–12. https://doi.org/10.1016/j.gsf.2014.03.004.

[57] Cheng, J., Xu, C., Xu, X., Zhang, S., & Zhu, P. (2025). Modeling seismic hazard and landslide occurrence probabilities in northwestern Yunnan, China: exploring complex fault systems with multi-segment rupturing in a block rotational tectonic zone. Nat. Hazards Earth Syst. Sci., 25: 857–877. https://doi.org/10.5194/nhess-25-857-2025.